Practical aspects of functional MRI (NMR Task Group #8)

Ronald R. Price[a)]
Vanderbilt University Medical Center, Department of Radiology and Radiological Sciences, Nashville, Tennessee 37232-2675

Jerry Allison
Medical College of Georgia, Department of Radiology, 1120 15th St., Augusta, Georgia 30912

Richard J. Massoth
Medical X-Ray Center, PC, 1417 S. Minnesota Ave., Sioux Falls, South Dakota 57015

Geoffrey D. Clarke
University of Texas Health Science Center, Department of Radiology, 7703 Floyd Curl Drive, Room 639F, San Antonio, Texas 78284-7800

Dick J. Drost
St. Joseph's Health Centre Nuclear Medicine & MRI Department, 268 Grosvenor Street, London, Ontario, N6A 4L6, Canada

(Received 23 January 2002; accepted for publication 29 May 2002; published 29 July 2002)

Functional MR imaging (fMRI) based upon the Blood Oxygen Level Dependent (BOLD) effect is currently an important new tool for understanding basic brain function and specifically allowing the correlation of physiological activity with anatomical location without the use of ionizing radiation. The clinical role of fMRI is still being defined and is the subject of much research activity. In this report we present the underlying physical, technical and mathematical principals of BOLD fMRI along with descriptions of typical applications. Our purpose in this report is to provide, in addition to basic principles, an insight into the aspects of BOLD imaging, which may be used by the medical physicist to assist in the implement of fMRI procedures in either a hospital or research environment.
 [DOI: 10.1118/1.1494990]

Key words: functional Magnetic Resonance Imaging, BOLD Effect, fMRI

I. THEORETICAL BASIS

A. Introduction

Magnetic Resonance Imaging (MRI) offers the ability to noninvasively image anatomic structures. This ability has been significantly enhanced since the first description of proton MRI by Paul Lauterbur in 1973.[1] The development of MRI as a clinically and scientifically useful tool has continued with little sign of reduced potential for further application. One of the more recent developments in MRI has been the ability to correlate the functional performance of biological tissues with anatomic location in a living organism.

There are several methods by which magnetic resonance can provide functional information on the status of living tissue. The function of biological systems is related to the intra and extracellular environment of the cells that make up the system. The phenomenon of magnetic resonance can be used to noninvasively probe the intra and extracellular environment. The use of MRI to detect pH and temperature differentials has been exploited in research applications, but not widely in clinical applications. Proton Magnetic Resonance Spectroscopy (MRS) is now used in both research and clinical settings to provide information on cellular function, tissue viability, tumor assessment, and differentiation between various pathologies. Contrast enhancement agents have been very effectively used to enhance the visualization of blood–brain barrier disruptions, allowing the assessment of clinical pathologies. Contrast enhancement agents are also used in imaging of blood flow (Magnetic Resonance contrast-enhanced angiography) and in imaging tissue perfusion. A critical issue is to define functional imaging in the context of this report. In this report we will consider functional imaging of the brain by the technique of MRI.

B. What is functional MRI (fMRI)?

Functional MRI (fMRI) could be defined as the use of a variety of techniques to correlate the physiologic activity of a tissue with its anatomic location. Clinical applications employ either endogenous or exogenous contrast agents. In MRI, the effects of contrast agents are detected indirectly through changes in the local signal intensity of specific pulse sequence protocols. The changes in local signal intensity arise as a result of changes in either the local relaxation rates, or in some cases the magnetic susceptibility effect of the agent. The most common exogenous contrast agents in clinical use are gadolinium complexes such as Gd-DTPA, Gd-DOTA, and other gadolinium chelates. Other exogenous contrast agents used in research applications include a variety of paramagnetic ions or particles, including lanthanide or dysprosium contrast agents, iron oxides, and superparamagnetic particles. In modern application, exogenous contrast agents are used either as first-pass or equilibrium contrast agents. In equilibrium applications, exogenous contrast agents are distributed in the extracellular compartment of tissues with a

disrupted blood–tissue barrier. Tissues with a disrupted blood–tissue barrier include a variety of neurological conditions such as vascular abnormalities and neoplasms. The longitudinal relaxation time constant, T1, of such disturbed tissues will be dramatically altered by the accumulation of the contrast agent, causing a change in the appearance of MR images. The tissue T1 is shortened primarily through dipole–dipole interactions between water protons and the unpaired electrons of the Gd ions in the contrast agent. The transverse relaxation time constant, T2, is also affected by the contrast agent, but the T2 effect is small until large local concentrations of the agent reduce the T2 of water by shortening diffusion in the locally inhomogeneous magnetic fields around the paramagnetic ions. The clinical doses of exogenous contrast agents administered are sufficiently small to avoid toxic effects from the contrast agent and any potentially free paramagnetic ions released from the agent. The clinical dose level is also in the regime where the effect on tissue contrast is approximately linear with concentration of the contrast agent. At significantly higher doses, the change in tissue contrast would no longer be linear with concentration.

In one type of fMRI, perfusion MRI, exogenous agents are typically used in a first-pass bolus experiment where an induced susceptibility change is desired. Susceptibility differences lead to local magnetic field gradients, which, in turn, contribute an additional component that accelerates transverse magnetization dephasing. The combination of irreversible T2 dephasing and the reversible dephasing due to local gradients is referred to as T2* (T2-star). A rapid imaging sequence sensitive to changes in T2* is employed to track the time course of signal loss and recovery caused by the transit of a bolus of the paramagnetic material through the local vasculature. As increased blood supply is expected in active regions of the brain, a greater signal loss is expected in regions that are more active. fMRI studies with an exogenous agent then may consist of mapping blood volume or flow differentials between a resting state and a task-activated state. In current clinical application, the contrast bolus is used to probe for irregularities in tissue perfusion such as those seen in stroke or trauma.

The most important endogenous contrast effect is the level of blood oxygenation. It was recognized by Ogawa, Lee, and co-workers,[2] that the amount of deoxyhemoglobin present in vessels affects the tissue contrast immediately around the vessel. The contrast effect is caused by the differential magnetic susceptibility of fully oxygenated hemoglobin as compared to deoxygenated hemoglobin in the blood. Oxygenated hemoglobin is less paramagnetic than deoxyhemoglobin. Cortical activation actually results in an increase in oxyhemoglobin concentration in the venous blood near the active cortex. As a result, magnetic susceptibility decreases and the T2* signal increases. Thus, the essence of fMRI is a functional map of the brain derived from the difference between images acquired with and without an activation stimulus. Since oxygen delivery, blood flow, and blood volume all increase with increasing cellular metabolism, the use of oxy/deoxyhemoglobin contrast effects offers great potential for functional imaging. Also, since no exogenous agents are used, the study can be repeated many times *in vivo*.

For the purpose of this report, we will focus on fMRI involving the use of endogenous contrast to correlate function with anatomy. In this report we will focus on functional imaging of the brain, an area of intense interest; however, functional MRI (fMRI) in organs other than the brain is also a current area of active research.

C. Historical development of fMRI

The basic concepts on which fMRI relies date to the late 1940s. The fundamental concepts of the nuclear magnetic resonance (NMR) signal loss by proton diffusion in the presence of a magnetic field were worked out at that time. NMR indicator dilution techniques were developed somewhat later, but well before the development of MRI. The physiologic principles of blood flow and volume measurements are over 100 years old and are based on indicator dilution methods involving dyes. The development of fMRI required advances in imaging hardware, software, and pulse sequence design as well as the development and characterization of MRI contrast agents and an adequate understanding of the mechanisms of contrast changes with blood oxygenation.

From studies in solutions by Thulborn *et al.*,[3] and work reviewed by Brooks and DiChiro,[4] it was established that local susceptibility changes in blood result from the intrinsic paramagnetism of deoxyhemoglobin in blood. The work of Ogawa, Lee, and co-workers,[2,5] showed that in high-field, high-resolution MRI, the image contrast surrounding blood vessels is related to the level of blood oxygenation in the vessels. Ogawa and Lee[5] suggested that this effect, now known as Blood Oxygen Level Dependent (BOLD) contrast, could be used to assess and monitor regional changes in tissue oxygenation. This was demonstrated in cats by Turner, LeBihan, Moonen, and co-workers in 1991,[6] and in rats by Ogawa and co-workers.[7] Although the susceptibility effects are smaller in current generation clinical MRI systems as compared to high-field research MRI systems, it is still possible to detect changes in the capillary and venous concentration of deoxyhemoglobin between resting and activated states, as shown in humans by Kwong, Belliveau, and co-workers.[8] Interest in fMRI escalated in 1992, filling scientific sessions and the proceedings of MRI meetings with functional activation studies involving motor skills such as finger tapping, as well as audible and visual recognition tasks. The importance of the emerging technique of fMRI was underscored by the 1993 Workshop on fMRI of the Society of Magnetic Resonance in Medicine (SMRM) held in Arlington, VA.

Positron Emission Tomography (PET) studies had shown that changes in neuronal activity are accompanied by local changes in cerebral blood flow (CBF),[9] cerebral blood volume (CBV),[10,11] and blood oxygenation.[12–14] Beliveau, Rosen, and co-workers[14,15] demonstrated that rCBV (r = regional) changes associated with neuronal activation could be localized with fMRI.

D. Principle aspects of BOLD contrast

Hemoglobin is a 64 500 molecular weight iron-containing protein that binds up to four oxygen molecules per hemoglobin molecule. Hemoglobin has two protein subunits: the protein globin and the iron-protoporphyrin complex known as heme. The attachment of oxygen to hemoglobin is dependent on the local oxygen partial pressure. The shape of the hemoglobin oxygen dissociation curve is sigmoidal; oxygen is bound more strongly when one or two oxygen ions are already bound than when no oxygen ions are bound. Conversely, when the oxygen partial pressure around the hemoglobin molecule is decreased then dissociation will more readily occur when one or more oxygen ions have been released. Only a very small amount of the directly dissolved oxygen in blood at normal microvascular pressures is paramagnetic ^{17}O, so the contribution to the relaxation rate of blood is quite small, on the order of 0.02 s^{-1}. The largest contribution to the relaxation rate of blood is from the deoxygenated hemoglobin or deoxyhemoglobin (dHb). Deoxyhemoglobin is very paramagnetic because the heme iron is in a high-spin ferrous state in which four of the six outer electrons are unpaired. The unpaired electrons have very large magnetic moments and associated paramagnetic properties. The attachment of an oxygen ion to the heme produces a sharing of the unpaired electron with the oxygen ion, which reduces the magnetic moment and associated paramagnetic properties. Fully oxygenated hemoglobin (Hb) has all of the unpaired electrons shared with oxygen ions, so the heme iron is in a low spin state with no magnetic moment or paramagnetic effects.

The bulk relaxation of blood is similar to the relaxation of Hb in solution; however, dHb is relatively inefficient in causing direct T1 relaxation because there is relatively little physical access for solvent water molecules to the unpaired electrons of the high-spin iron in the heme of ordinary hemoglobin. The bulk relaxation effects of the red blood cell (RBC) cellular membrane and plasma proteins appear to be limited.

The applied magnetic field causes the paramagnetic iron in dHb to reinforce the external field and produce a relatively larger local field because of the susceptibility of paramagnetic dHb. Since dHb is confined within the cellular membrane of RBCs, the average susceptibility is inhomogeneous, leading to a highly inhomogeneous local magnetic environment. Since there is no motional component at frequencies near the Larmor frequency to promote energy transfer, the field inhomogeneity does not affect T1 relaxation rates. However, proton T2* relaxation is affected by the motion of protons in the inhomogeneous local magnetic fields, so that spins lose phase coherence at rates depending on the local magnetic field inhomogeneity.

The susceptibility of fully deoxygenated RBCs is 0.2 ppm greater than fully oxygenated blood.[3,4] Field mapping results from Weisskopf and co-workers[16] show that there is a linear relationship between susceptibility and blood oxygenation at 1.5 T. The relative susceptibility difference between paramagnetic dHb within the RBCs and the surrounding environment produces local regions of an inhomogeneous field. Diffusion models are used to describe the effects on MRI signals caused by the diffusion of water protons through the inhomogeneous field. The diffusion models make assumptions as to the spin exchange between the different local field environments and the relative contributions of water diffusion through the intracellular, extracellular, or transmembrane field gradients on the observed changes in the T2* relaxation rate.

Ogawa, Lee, and co-workers[2] first demonstrated at high field (7 and 8.4 T) and high resolution (65 μm pixels) that changes in paramagnetic dHb levels can be correlated with local blood flow and local brain activity. They coined the term ''blood oxygen level dependent'' (BOLD) contrast to explain the phenomenon. The image contrast correlated well with the oxygen level in the breathing mixture administered to rats. Under normoxic conditions, BOLD contrast reflects the status of the venous microvasculature of the brain.[17] The subtraction of images with and without an activation stimulus can be used to obtain functional maps of the brain.[18] The association of an activation-induced signal with local dHb levels is supported by the lack of significant contrast changes with the introduction of carbon monoxide into breathing mixtures since carbon monoxyhemoglobin is not paramagnetic but still lowers the local oxygen pressure.

There is a field dependence on BOLD contrast that was investigated by Turner and co-workers.[19] They compared the results from visual stimulation at 1.5 and 4.0 T under similar experimental conditions. The observed mean change in signal intensity was approximately 15% at 4 T and approximately 4.7% at 1.5 T. The T2* relaxation rate is linearly related to the level of oxygen saturation.[7] A calibration curve can be constructed to allow noninvasive measurements of oxygen pressure in venous blood using a conventional clinical MRI system, as shown by Wright.[20] The susceptibility-induced frequency difference between the Hb and dHb inside of the RBCs and the surrounding environment depends on the strength of the applied magnetic field. Thus, the inhomogeneous field contribution to signal decay will depend on the applied magnetic field. The bulk T2* of both oxygenated and deoxygenated blood varies approximately quadratically with external field strength, as shown by Thulborn *et al.*[3] and Gomori *et al.*[21] in measurements that span 8–469 MHZ. Brooks and DiChiro imaged blood samples with varying oxygenation states at 1.5 and 0.5 T to find that the dHb contrast is greater at 1.5 T than would be expected at 0.5 T by a linear model. Simulation studies by a number of groups[22,16,18] using the model of vessels as paramagnetic cylinders predict that for constant echo time the T2* relaxation rate change for a change in blood susceptibility should vary as the 1.6–2.0 power of the static B_0 magnetic field.

Vessel size plays an important role in the source of signal in fMRI sequences. The source of signal in spin echo fMRI studies is primarily from capillaries. Simulation studies indicate that vessels of diameters less than 30 μm dominate contrast in spin echo sequences. The source of the signal in a gradient echo sequence is from larger venules and veins as well as capillaries.

The image signal-to-noise ratio (SNR) generally increases with increasing field strength. However, Jezzard *et al.*[23] showed that *in vivo* background noise in gray matter during fMRI experiments (not including motion and hardware instabilities) at 1.5 and 4 T are very similar. Thus, image noise sources are not particularly field dependent, which implies that the dominant noise source is not electronic, but is physiologic.

The signal change with blood oxygenation depends on the change in blood susceptibility and the vessel volume fraction in each imaged voxel. Ogawa and co-workers[18] suggest that venous oxygen saturation dominates all other factors. At 7 T in rats, Ogawa and Lee[4] show that blood oxygenation changes from 0% to 100% produce a gradient echo (TE $=15$ ms) signal change of 15%–20% in regions devoid of obvious large blood vessels. Under similar conditions, spin echo signals change only a few percent. During photic stimulation at 1.5 T, Kwong *et al.*[8] found by simulation that tissue with an initial blood volume fraction of 4% should show a 2% signal increase in GRE (Gradient Referred Echo) images (TE$=40$ ms). This matched their experimental results of primary visual cortex signal changes of $1.8\% \pm 0.8\%$ with visual stimulation. The simulations of Kwong *et al.*[8] assume that blood volume increases by 30% and flow increases by 70% during activation. Other groups[19,24–27] report average signal changes of 1%–6% with gradient echo images in the 1.5–2.0 T range and 5%–20% with 4 T systems.

The results of fMRI studies with EPI (Echo Planar Imaging) systems show that signal intensity changes are observable within seconds of the onset of activation by stimulation. The latency of activation-induced BOLD in primary cortical regions of the brain is in the range of 5–8 s (to 90% of the maximum signal change) following stimulus onset and in the range of 5–9 s (to 10% of the maximum signal change) following removal of the stimulus.[8,28,29] Often a transient undershoot is seen at the end of each stimulation cycle. Also, on occasion, a decrease in baseline value is observed after the first activation cycle.[25] The increase in signal intensity is probably caused by transient hyperoxemia and increased local blood volume caused by regulatory overcompensation by the local circulatory system, similar to mechanisms proposed in PET studies. The observed fMRI signal rise times is in reasonable agreement with cerebrovascular transit time measurements with ^{15}O-labeled carboxyhemoglobin.[30] The rise times may represent the vascular transit times for the involved tissue.[8] However, the majority of the activation-induced T2* change should not be detectable until the blood has transited the capillary bed and the relatively more oxygenated blood fills the venules. In animal studies, Turner and co-workers[6] demonstrated that signal intensity changes were observable within seconds of reduction in blood oxygenation induced by changes in the breathing mixture. The observed signal change occurred at 6 s and presented a distinct overshoot upon the restoration of a normal breathing mixture. Turner *et al.* suggest that the overshoot indicates a transient decoupling between blood flow and oxygen utilization after restoration of normal oxygen levels in the breathing mixture. It has been reported that CBF is enhanced during temporary anoxia,[31] and there may be a temporary excess oxygen delivery upon return to normoxia. However, the depression of metabolism during anoxia may transiently persist following return to normoxia. The basal level of arterial oxygen saturation is close to maximal, as shown by Turner *et al.*,[32] and the observed signal overshoot during recovery is not likely to reflect arterial dHb levels.

E. Clinical utility of fMRI with BOLD

Since the introduction of BOLD contrast in MRI by Ogawa and co-workers[2] in 1990, a rapidly increasing number of studies have been published, employing this method of studying function. The first areas of the brain investigated were the visual and motor cortices.[8,24,33,34] Attempts to study other brain regions have been made with varying success, primarily because of technical difficulties and especially because the accuracy of the localization is called into question. Localization refers to the discrepancy between where neurons are activated and where the decrease in dHb occurs in the brain. The issue of whether the enhanced signal occurs primarily in the intravascular or extravascular space is also still hotly debated.[35–41] In this section we summarize a few of the clinical applications.

Visual stimulation was one of the first areas to which BOLD fMRI was applied. A large portion of the cerebral cortex is involved with vision, so there is a large area of activation. The initial procedures were developed by Belliveau and co-workers.[11,42,43] Preliminary results[44] demonstrate that fMRI can delineate deficits in activation of the visual cortex that are consistent with clinical field deficits.

Motor and sensory area mapping has been studied by PET and other techniques, so it has been an area of extensive fMRI work. Results of motor/somatosensory mapping studies are consistent with reports from PET, including activation patterns from isotonic hand flexion/extension or electrical stimulation of the wrist as well as asymmetric motor activation patterns caused by handedness. Rao *et al.*[34] mapped the primary motor cortex locations for fingers, toes, elbows, and tongue. fMRI was compared to conventional invasive mapping procedures as part of a neurosurgical planning process by Jack *et al.*,[45] Hirsch *et al.*,[46] and Lin *et al.*[47]

From earlier non-MRI work, it is known that there is a tonotopic organization of blood flow responses to varying tonal frequencies. Hemispheric activation occurs contralaterally to the ear that receives the tonal stimulation. Auditory experiments have not been as vigorously pursued because of the anticipated competition from the loud and repetitive sounds produced by the imaging gradients. Despite the fact that the gradient system noises are much louder than the stimulus responses, several groups report fMRI studies of auditory stimulation.[48–50] The earliest brain mapping work by neuroanatomists involved the language and speech areas of the brain. Mapping of these areas is important in neurosurgical planning to minimize damage to these important regions of the brain. As the limited spatial resolution of Single Photon Emission Computed Tomography (SPECT) and PET limit their usefulness in determining activated regions in lan-

guage and speech processing, fMRI is of particular interest to neurologists. Language lateralization has been demonstrated by fMRI during internal word generation tasks in adults[47] and children.[51] A variety of mental tasks have also been studied by fMRI.[52,53]

In clinical applications epilepsy, stroke, pain, pharmacologic intervention, obsessive–compulsive disorder and Alzheimer's disease have all been studied with fMRI. Brain reorganization following stroke[54,55] and in patients with intracerebral tumors[56] and following surgical intervention[57] are all active areas of investigation.

II. HARDWARE REQUIREMENTS

Typical fMRI studies are done with a T2*-weighted EPI sequence acquiring images at a rate of 10 images/second for about 5–10 mins. Since a 128 squared matrix with a 250 mm FOV is ideal, this requires gradient rise times on the order of <300 μs for 25 mT/m. Other requirements include the following.

A. Computer system

A computer system capable of acquiring, reconstructing, and storing 3600–18 000 images per fMRI study. Most current commercial MRIs cannot do this without some system manipulation by an expert user. Image reconstruction, data transfer, and fMRI image processing are very time consuming. Although modern MRI scanner computers can now reconstruct several thousand images in minutes, transferring these images to an off-line computer station for fMRI processing will take more than an hour over a typical hospital network with an effective throughput of 1 Mbit/s. State of the art computer hardware will have no problem processing this data, but the required user inputs and checks can add hours to days before useful results are produced.

B. Shimming

Since strong T2* weighting is required, the center of *k* space should be acquired at about 40–to 60 ms (at 1.5 T). This, in turn, requires a very good shim for a sufficient image signal to noise and, therefore, ideally a shim set under control of a computer having an automated shimming algorithm. With a second-order shim set and a shimming algorithm, a T2*$>$60 ms at 1.5 T and $>$30 ms at 4 T can be achieved. In theory, the optimum TE times would be 60 ms at 1.5 T and 30 ms at 4 T, but in practice slightly lower echo times are usually more optimum since pixel noise from image to image increases at later TE times because voluntary or involuntary patient motion causes changes in field homogeneity.

C. Stability

It has been demonstrated that a 0.3% standard deviation for a repeated single EPI image acquired every second for about 0.5 h is possible. Images were acquired on a phantom, using a ROI large enough that image noise was much less than 0.3%. Since the BOLD effect is small, signal stability is extremely important. This puts very strict requirements on radiofrequency (rf) transmitter stability, phase and gain stability of the receiver, gradient driver and gradient coil stability (thermal effects in the gradient coil), shim power supply stability, and magnet field drift stability. One more generation of MR hardware development may be required to reach 0.1% standard deviation for images acquired over the time course of a fMRI study.

Since post-processing requires some type of image ''subtraction,'' spatial stability of the images is important. The image should not move or distort by more than a pixel during the data acquisition period. Again this puts very stringent performance requirements on the gradient and shim hardware. Auto-registration of images during post-processing may be required, which adds to the computer processing time mentioned in Sec. II A). Since the brain moves under CSF pulsations, cardiac triggering may also be desirable. Although site visits can determine signal and spatial stability on phantom tests, the installed system stability may be limited by siting problems; building vibration, magnet room temperature fluctuations, and chilled water supply temperature fluctuations, for example, can all increase the instability of the final image.

D. Immobilization

Some type of patient restraint device is required. Wedges around the patient's head with foam pieces between the head and the head coil are a minimum requirement. Since the patient may have to speak or move his hand(s) to use a computer joystick to carry out a fMRI algorithm, there may be diminishing returns on very sophisticated restraining devices. Patients are often anxious and may be claustrophobic. The use of rigorous head restraint for these patients can be self-defeating. Good communication and prepping of these patients is critical for obtaining good fMRI results and can be more important than rigorous head restraint. Also, as found with MRS studies, even if the head is constrained the shim may change when the patient moves their legs or arms. A total body restraining device would not be considered patient friendly. (Since the patient or research subject may be in the magnet for 1–2 h, subject comfort is more important than for conventional imaging.) There may be diminishing returns since brain motion from CSF pulsations and shim changes due to patient breathing ultimately dominate voluntary patient motion or hardware drift.

E. Task presentation systems

In order to conduct fMRI studies, a task presentation system is necessary. Depending upon the nature of the task, a computerized stereo sound system for aural input and a visual presentation system may be required. In order to document whether the patient is doing the task, a keypad, joystick, or trackball system to record patient response to selected stimuli may be required. Task presentation apparatus is commercially available, but most studies to date have been done with an apparatus adapted by individual institutions to fit the needs of their particular tasks. For nonvisual tasks, it is desirable to turn off the room lights and magnet bore lights and have the patient close their eyes in order to eliminate

confounding activation of a visual cortex. Visual presentation systems range from a simple 35 mm slide projection to liquid crystal display panels to sophisticated electronic goggles. For visual data containing fine detail, MRI compatible corrective lenses may be necessary. Task presentation systems, physiologic monitoring, and patient response monitoring should be in synchrony with the acquisition of the T2*-weighted images acquired in a fMRI study. Ideally, all of this apparatus should be controlled by one host. Wires and tubes associated with a fMRI study must pass into and out of the MRI exam room through rf filters or rf waveguides.

Since some fMRI algorithms use audible stimulation, gradient noise is an important concern. Earphones with significant acoustic attenuation (commercially available up to 30 dB) can generally be used as part of the audio communication equipment.

III. PULSE SEQUENCE CONSIDERATIONS FOR FUNCTIONAL MRI

Practically every type of pulse sequence used for MRI can be adapted for fMRI, with the appropriate modification of resolution and contrast parameters. Therefore, we begin with a brief review of pulse sequence features. We then summarize each pulse sequence type used for fMRI and list its particular strengths and weaknesses.

A. Overview of pulse sequence classification by *k*-space trajectories

MRI is unique among medical imaging modalities in that the raw data is sampled in reciprocal space. For Fourier transform MRI this means that the data is sampled and then an inverse Fourier transform is performed in order to produce a matrix in which the intensity of each element corresponds to the signal obtained from a linearly mapped position in space (the image). Thus, MRI imaging schemes can be broadly classified by the path or trajectory in which the reciprocal *k* space is sampled.

Unlike normal space, *k* space exhibits conjugate symmetry about the center point that represents zero spatial frequency. The signal magnitude is typically maximum very close to this center point as large structures dominantly contribute to the signal power. Because the entirety of *k* space is not sampled instantaneously, conjugate symmetry of the MRI signal in reciprocal space may be lost in practice due to time-dependent processes that affect the MR signal. Two-dimensional representations of *k* space are shown in Fig. 1, with sampling trajectories for several classes of pulse sequences depicted. A short radio frequency (rf) excitation pulse followed by data acquisition with a single, constant B_0 gradient will cause the signal to begin in the center of *k* space. This scheme was used by Lauterbur in his projection reconstruction method of MRI [Fig. 1(a)], but is generally too slow for fMRI. Pulsed magnetic field gradients determine the *k*-space trajectories. Readout gradient reversal reverses the signal trajectory in the k_x direction.

A phase-encoding gradient pulse will move the signal a predetermined amount in the k_y direction. This forms the basis of the spin warp 2-DFT method depicted in Fig. 1(b). A 180° refocusing rf pulse can reverse the change in phase of the MRI signal, which is useful for producing rf spin echoes (SE) that are relatively insensitive to B_0 inhomogeneities. In *k* space this has the effect of transporting the signal sampling to the spatial frequency point, which is the complex conjugate of the original position in *k* space. In fast spin echo methods, this approach is used to speed the imaging process by acquiring several lines of data during multiple echoes following one rf excitation [Fig. 1(c)]. If the magnetic field gradients are strong enough and can switch rapidly many lines of *k* space may be sampled before the MRI signal decays excessively due to T2.

Blipped echo planar imaging allows one to scan an entire low resolution image in very short imaging times. Use of echo planar imaging with a sinusoidal readout gradient waveform and continuous data sampling [Fig. 1(d)] requires that special image processing steps must be introduced since the Fourier transform expects to see the data points sampled on a rectilinear grid. Image reconstruction in spiral scanning, which uses oscillating gradients with data sampling moving outward from the center of *k* space [Fig. 1(e)], is also computationally intensive.

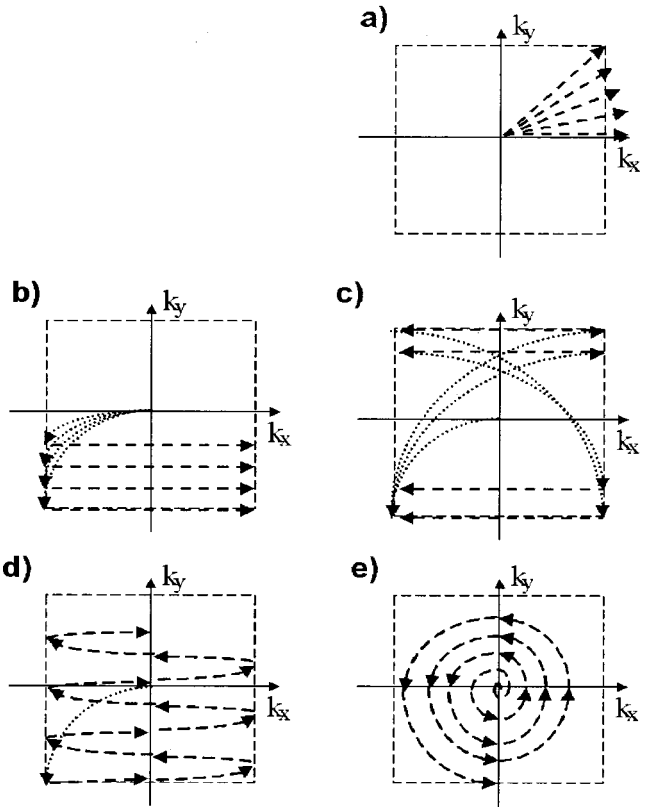

FIG. 1. (a) *k*-space trajectories for various MR imaging schemes. Projection reconstruction starts at the center of *k* space for each excitation. (b) In spin warp MRI, the magnetization is moved to the corner of *k* space and one gradient echo or rf spin echo line is scanned for each excitation. (c) Fast spin echo, starts as in (b), but multiple 180° pulses bounce magnetization to complex conjugate positions in *k* space with multiple lines (echoes) acquired for each excitation. (d) Blipped EPI traverses all of *k* space from one excitation pulse. (e) Spiral scan MRI starts similarly to (a) but oscillating gradients cause *k* space to be scanned in one or more spiral trajectories.

TABLE I. Typical pulse sequence parameters for spin warp/gradient echo fMRI studies. At higher field strengths the cerebral activation effects on the MRI signal are more apparent.

Main field	Flip angle	FOV (mm)	Matrix size	Slice th. (mm)	TR/TE (ms)	Slices	Image time	Stimulation	Ref.
1.5 T	25°	200	128×256	4	67/40	1	8.58 s	motor	25
2.0 T	40°	200	64×128	8	47/38	1	3.01 s	photic	39
4.0 T	11°	299	64×128	10	9.6/6	3	0.61 s	photic	27

B. Contrast and resolution parameters in MRI

Signal intensities are modulated by T2 and B_0 field inhomogeneities (collectively called T2* effects) and by eddy currents created by the gradients. Radiofrequency pulses and appropriate delays are used to change image contrast by manipulating the relative amounts that proton density and T1 recovery contribute to the MRI signal. In fMRI, using BOLD contrast, we are generally attempting to identify active brain regions based on T2*-weighted MRI techniques.

The desire to enhance susceptibility effects limits the use of the inhomogeneity insensitive rf spin echo sequences. Therefore, gradient-echo sequences, either FLASH (Spoiled GRASS) or EPI, are used with TE times from 20–60 ms to provide strong T2* weighting.

Since the BOLD effect increases as the main B_0 field is increased, there is expanding interest to perform fMRI studies in 3–4 T magnets. Since tissue T2* also decreases with B_0, TE times are also decreased with B_0 to obtain the optimum contrast/noise ratio in fMRI.

Structural T1-weighted MRI images are usually acquired on each patient. It is advantageous to acquire a volume or 3-D dataset having roughly isotropic voxels. This facilitates reformatting the 3-D dataset into oblique images that have the same geometry as the fMRI datasets.

In language-oriented studies, it is desirable to image the entire brain since activation will occur in several areas of cerebral cortex. On conventional MRI systems, there is generally a tradeoff between slice thickness, the number of slices, and the number of measurements. While it is advantageous to have very thin slices (~3 mm) to minimize intravoxel dephasing and partial volume effects, this may require up to 32 tomographic slices to cover the 10–14 cm extent of the brain acquired in transverse–oblique or sagittal imaging. The acquisition of 32 slices per measurement may limit the number of measurements in a fMRI protocol. For example, 16 tomographic slices encompassing the entire brain are acquired every 3 s for 6.4 min would produce 2048 images. Thus, each tomographic slice will be acquired 128 times during the study and each volume element (voxel) will have a voxel time course of 128 data points acquired at 3 s intervals. During data acquisition, the fMRI task is usually alternated every 10–30 s. The alternation of activation and control tasks reduces boredom or habituation and affords better correction and compensation for hardware drift and patient motion.

C. Imaging speed

It is imperative that little motion occurs between the baseline and activated image data acquisitions since BOLD contrast is obtained by subtracting a ''baseline'' dataset from some activated dataset. Thus, it is highly advantageous to obtain fMRI datasets in the shortest possible amount of time. This also adds temporal information to the activation response. For single-slice fMRI, a gradient-echo sequence has adequate speed, but multislice fMRI requires EPI.

D. Spin warp imaging methods

Spin warp imaging methods are commonly employed on all commercial MR scanners. In these, one phase-encoding line of data is acquired for each rf excitation. After the rf pulse nutates (or tips) the net magnetization vector into the transverse plane the spins begin dephasing due to T2 relaxation, the applied imaging gradients and the effects of local B_0 field inhomogeneities. A reversal of the imaging gradient field causes the spins to rephase and produces an increase of signal (this is called a ''gradient echo'' or ''field echo''). Note that the signal is still partially attenuated since the dephasing effects of T2 relaxation and local B_0 field inhomogeneities have not been reversed. When partial flip angle excitation is used in conjunction with a refocusing readout gradient set for a TE of about 60 ms at 1.5 T, an image is obtained with adequate SNR and strong signal dephasing due to magnetic field susceptibility differences. This strategy is employed because it is desirable to enhance the dephasing due to magnetic susceptibility differences in activated and quiescent tissues. This approach can be carried out in brain tissue since the T2 values are relatively long and do not cause the signal to disappear before magnetic field susceptibility attenuation becomes appreciable. Also, because these gradient-echo sequences are dependent on T2* contrast, the images are sensitive to other sources of magnetic field inhomogeneities and susceptibility artifacts. Susceptibility artifacts near soft tissue/air interfaces and soft tissue bone interfaces are very apparent in images acquired using long-TE gradient echo sequences.

Typical gradient-echo (GE) pulse sequence parameters, as reported in the literature are listed in Table I.

Conventional gradient-echo sequences allow better spatial resolution than faster EPI pulse sequences (see below). They are more readily available on conventional MRI systems. An echo shifted variant has been proposed to allow increased

effective echo time without increased TR.[58] Another variant uses a magnetization preparation technique to reduce the time required to obtain multiple slices.[59] A low bandwidth/long readout time should be used to increase the SNR, which will also require good shimming.

E. Fast spin echo imaging (FSE)

Gradient reversals do not effect the decay of the MRI signal that is attributable to T2 relaxation and the effects of local B_0 field inhomogeneities. In order to preserve more signal, a family of special rf pulsing schemes, called spin echoes, have been developed to minimize the effects of magnetic field inhomogeneities. To produce a spin echo, the net magnetization vector is nutated through 180° before it has a chance to completely dephase. The orientation of the magnetic fields become reversed from the spins' frames of reference and those spins that once were dephasing begin to rephase.

Many MRI examinations are hindered by the natural physiologic motion of organs or involuntary patient motion. Instead of acquiring only one line of data for each excitation pulse, fast imaging methods have been developed that enable multiple lines of data to be sampled from one excitation pulse. One of these sequences, called Fast Spin Echo, utilizes multiple 180° refocusing rf pulses to produce Hahn echo signals that refocus more signal than simple gradient reversals.

As long as T2 is adequately long, multiple 180° pulses can be applied that refocus the transverse magnetization at regular intervals. This sequence of 180° rephasing pulses produces multiple spin echoes. In *k* space, each 180° refocusing pulse moves the transverse magnetization vector to its complex conjugate position. Thus, combined with appropriate gradient switching, a different line in *k* space may be scanned for each of the multiple echoes produced. FSE does not require very strong, fast-switching gradients, but does work most robustly in situations where there are minimal eddy currents.

The practical disadvantage of using multiple 180° refocusing rf pulses is time. Since additional time must be included for the application of these rf pulses and their associated slice select gradients the echo time (TE) must be longer than for a simple SE sequence.

Fast spin echo methods have been proposed for fMRI because the signal produced by these schemes is relatively free of signal from large vessels. These large vessels, which tend to lie along the surface of the cerebral sulci, can confound the interpretation of fMRI data obtained using gradient echoes. However, FSE images have less susceptibility weighting and thus the changes seen in the images during activation are primarily due to the increased water diffusion occurring during mental tasks.

Two groups have investigated the use of FSE for fMRI. They report signal-to-noise benefits that help to compensate for the relative decrease in the differences between baseline and photic stimulation images.[60,61] (See Table II.)

TABLE II. A typical FSE fMRI imaging sequence at 1.5 T.

TR	TE_{eff}	Echo train length	FOV	Matrix	Averages
2500 ms	100–200 ms	16	40 cm	128×256	2

Since photic stimulation produces one of the largest activation effects observed, other more subtle activation protocols may not be able to take advantage of FSE imaging schemes.

The use of conventional spin echo, fast spin echo (FSE), and gradient-echo techniques will limit the production of fMRI images to a few topographic slices per study. This is not a severe limitation when imaging the activation along the motor strip associated with a motor task, but is unacceptable when surveying the entire brain for diffuse activation such as that associated with a language task. When surveying the brain, it is preferable to use single shot techniques that enable data collection for one topographic slice following a single rf excitation pulse. Single shot techniques are fast enough to acquire data for 16–32 topographic slices in a period of 3 s, thus enabling a survey of the entire brain every 3 s.

Conceivably, BOLD imaging sequences are not highly dependent upon temporal resolution because a first-pass phenomenon is not being observed, however, temporal resolution does become important when multislice or activation response time studies are desired such as event-related fMRI analysis. Temporal resolution in conventional spin echo and fast spin echo (FSE) sequences are primarily limited by rf power deposition considerations due to the number of rapid rf pulses required to acquire an image. Single shot EPI sequences can achieve the desired image acquisition speed and minimize rf power deposition. Temporal resolution in conventional gradient echo sequences is similar to the response times of the hemodynamic mechanism in BOLD fMRI. Gradient echo EPI imaging offers an improved signal-to-noise ratio (SNR) in shorter scan times because most of the equilibrium magnetization is available for manipulation (one 90° rf pulse instead of many smaller alpha pulses). In conventional gradient-echo sequences, only a fraction of the equilibrium magnetization is available due to the saturation of steady-state magnetization created by multiple rf excitation.

F. Echo planar imaging

Echo planar imaging (EPI) approaches can be used to produce MRI images in the shortest amount of time.[62–64] EPI was proposed by Mansfield in order to acquire an entire image following a single rf excitation. Some images may be produced in less than 100 ms by moving the transverse magnetization through *k* space in a rasterlike fashion. Images of this type are snapshots of the anatomy at a given instant and have less artifact produced by patient motion. In order to produce an image for each rf excitation, the MRI system hardware must be significantly modified. EPI places increased demands on the functional capacities of the gradient, radiofrequency, and data processing subsystems. Improve-

TABLE III. Representative single shot EPI parameters for MRI studies. These studies are often limited by gradient coil capabilities and SNR. GE=gradient, echo EPI; TE_{eff}=effective TE; pulse sequence=rf pulsing mode.

Main field (T)	Pulse seq.	FOV (mm)	Matrix size	Slice (mm)	TR/ TE_{eff} (ms)	Read wave form	Image time (s)	Stimulation	Ref.
1.0 T	GE 90°	300	128×128	10	1500/ 160	bipolar sine	0.107	apnea	62
1.5 T	GE 90°	200	64×64	5	2000/ 50	bipolar sine	0.040	motor	63
1.5 T	30° GE	200× 400	128×256	5.0	3000/ 60	bipolar sine	0.080	perceptual	64
3.0 T	90° GE	240	96×96	8	2000/ 40	bipolar sine	0.100	motor	65

ments in temporal resolution are made at the expense of spatial resolution and/or signal-to-noise ratio (SNR). The SNR may be improved using signal averaging and spatial resolution may be increased by multiexcitation EPI schemes. However, these compromises necessarily increase the time per image. As shown in Table III, EPI approaches to fMRI usually have poorer spatial resolution and better temporal resolution than their conventional SE and gradient-echo counterparts. In designing the specific acquisition protocol for a fMRI task, the medical physicist is often constrained by the total number of images than can be acquired in one acquisition and the number of slices that can be acquired in the desired TR (which depends on the number of phase encodings per slice).

EPI is made possible by the use of fast-switching strong magnetic field gradients. Gradient systems that can achieve 25 mT^{-1} to greater than 40 mT^{-1} in 250–300 μs are available on the most advanced MRI scanners. EPI can be accomplished with slower switching gradients but only at the cost of reduced coverage (fewer slices), reduced spatial resolution, and reduced temporal resolution. Instead of using dephasing gradient pulses and sampling the signal once during a readout period following excitation, in EPI the readout gradient is reversed and data sampling occurs during both positive and negative readout gradient lobes [Fig. 1(d)]. This bipolar acquisition technique typically employs a sinusoidal gradient waveform that produces efficient gradient switching response but that results in motion through *k* space at a variable rate. To handle this problem data may be sampled at a concomitant variable rate by increasing the sample time around the maximum of the sinusoidal read gradient. In order to transform the data onto a rectangular *k*-space grid, the time integral of the gradient waveform is calculated, divided by the number of samples, and then sample times are chosen corresponding to the integration. An alternative to using nonuniform sampling is to use trapezoidal (square wave) readout gradient waveforms. These waveforms also have a finite rise time, which is often more difficult to characterize. Thus, when trapezoidal gradient waveforms are used, data sampling is usually, but not always restricted to the plateau, causing the data sampling window to be switched on and off.

Bipolar EPI data acquisition schemes require line-by-line phase (or time) shifts to be applied to the data before Fourier transformation in order to reduce or eliminate ghosting artifacts that generally occur at one-half the field of view (FOV). In addition, high magnetic field homogeneity is required. The operator must be able to shim the fields homogeneity over the body part under investigation to below 1 ppm. A MRI system with a second order room temperature shim set plus an automated shimming algorithm can typically achieve a global head shim $<$20 Hz FWHM. Second, a prescan algorithm, in which a sample image is acquired without the phase-encoding gradient turned on allows the operator to calibrate the degree of shifting required on a line-by-line basis. Third, eddy currents degrade the image by producing distortions and ghosting artifacts in the echo planar image. The use of self-shielded gradient coils and/or dynamic eddy current compensation significantly improves the fundamental quality of the EPI data.

Performing these line-by-line adjustments followed by the Fourier transformation of image datasets acquired every 100 ms is very computer intensive.[65] Most current imaging systems quickly reach their data processing limitations when even modest fMRI experimental protocols are implemented. Breakdowns may occur anywhere along the data path. Fundamental limitations include the amount of digitization memory, buffer sizes and architecture, bus bandwidths, and image display speeds. When performing sequential fMRI acquisitions consisting of 1500 images in 6 min, it may be necessary to wait for up to 15 min between studies for images to be reconstructed and written to disk. Some EPI scanners limit the maximum number of acquisitions and images that can be acquired in one fMRI study (e.g., 128 acquisitions and 512 or 2048 images). Additionally, fMRI postprocessing requires pixel by pixel subtraction from the reference image(s) and may include various segmentation and correlation algorithms, many of which require lengthy computations.

Echo planar imaging is distinguished by the remarkable flexibility it gives the investigator in preparing the magnetization before the activation task has begun. An example of this is the EPI-STAR approach proposed by Edelman *et al.*, in which a selective inversion rf pulse caudal to the imaging slice is used to label spins before they move cranially.[66] A

TABLE IV. Typical spiral scan MRI sequence timing parameters with a total imaging time of 6.4 s.

TR	TE	Flip angle	FOV	Matrix
50 ms	30 ms	30°	30 cm	128×256

number of investigators are currently using a variety of different arterial spin-labeling techniques to directly measure cerebral blood flow.[67–69] Several texts[70–73] and review articles[74] are available to those interested in the details of fMRI using EPI.

G. Projection reconstruction and spiral scan methods

In spiral MRI, a slice is first selected using a slice selection gradient and then the two gradients perpendicular to the slice-select gradient are oscillated at 90° out of phase. This causes the transverse magnetization to traverse *k* space in a spiral, ranging from the central, low spatial frequency portions outward. Spiral MR images are generally not acquired in a single excitation; several are used. However, proponents of this method have reported that it is more robust compared with conventional techniques (GE spin warp) with respect to motion artifacts,[75,76] and that the inherent flow compensation is advantageous for fMRI acquisitions. (See Table IV.)

Thus, this class of imaging is generally slower than EPI in terms of temporal sampling. More recent studies, however, have demonstrated similar acquisition rates with spiral sequences relative to EPI.

Apart from motion insensitivity, the spiral scan is attractive because one can achieve slightly better spatial resolution trading-off temporal resolution, yet using conventional MR system hardware. However, spiral scanning does require the development of special pulsing algorithms and additional post-processing to interpolate the data to the rectangular matrix expected by the Fourier transform. Thus, only a few groups are seriously pursuing this approach to fMRI.

H. Other innovations

In addition to the basic imaging schemes, outlined above, several investigators have proposed accessory methods to improve the ability of the basic pulsing methods in ways that will specifically benefit fMRI. Navigator echoes are prepulses used to measure the amount of motion occurring during the scan and are used to correct for motion artifacts. They have been applied to GE spin warp fMRI sequences.[77] Navigator echoes have also been used in combination with a multiexcitation EPI fMRI scheme.[78] Also, one group of investigators has proposed using keyhole imaging, in which only the low spatial frequency portions of *k* space are sampled rapidly.[79] Another approach using 3-D PRESTO can produce approximately 20 slices (128×64 matrix) with TE greater than 30 ms in a 6.5 s scan time. This method can be implemented on non-EPI hardware and facilitates 3-D motion correction in *k* space. Attempts have also been made to sample only the higher spatial frequencies based on the assumption that only small structures contribute to fMRI activations.

For most physicists trying to implement fMRI in a clinical setting, the pulse sequences to be used will be determined by the capabilities of the imaging hardware and the specific imaging packages provided by the MRI system vendors. Currently the GE spin warp method and single-shot EPI have been most commonly used. GE spin warp requires no special hardware or software (other than for post-processing). However, its temporal resolution is poor, and its use is limited to single slices. Although some EPI sequences are implemented on conventional scanners, the fastest EPI requires expensive upgrades to the standard imaging system.

This summary has been aimed at giving a general overview of methods currently under investigation for fMRI studies. Please consult the references for more details on how fMRI may be implemented in specific clinical settings.

I. Quality control

Since fMRI is sensitive to variations in signal intensity or image position, which results in an apparent intensity difference, an important QC test is to run the fMRI protocol on a phantom. This may require acquiring several thousand EPI images over a 10–20 min period. A large ROI is then placed over a uniform region in all the images and the mean signal within the ROI is then plotted as a function of all the images acquired for one slice position. A typical coefficient of variation (CV) for the ROI signal is 0.3% for a properly functioning MR system. There should be no drift and the constancy of the spatial dimensions and position of the phantom can also be tested by subtracting images selected at different time points from the first image and looking for edges. Changes in spatial position are usually caused by variations in B_o, which can be caused by temperature changes in passive shims or instabilities in the Z^2 shim. Single shot EPI is particularly sensitive to B_o shifts because of the low bandwidth/pixel ($\approx$ 10 Hz) in the phase encode direction.

IV. DATA ACQUISITION PROTOCOLS

Protocols for various activation tasks from several institutions are included in the Appendix for specific reference by the reader. Included are sequence timing parameters, image acquisition formats, a brief description of task and task presentation, along with some representative activation maps.

V. DATA ANALYSIS

The Blood Oxygen Level Dependent (BOLD) technique is accomplished by rapidly imaging through alternating periods of activation and control states. Relatively short periods of activation and control (5–30 s) are normally used to prevent response saturation (habituation or boredom), as well as to facilitate the use of bandpass filters to reduce low-frequency artifacts (baseline drift). In response to an activating task, several phenomena occur in or near the affected cortex: cortical activation occurs, metabolism increases, blood flow increases, blood volume increases, blood oxygen

extraction increases slightly, venous blood oxygenation increases, venous blood deoxyhemoglobin concentration decreases, blood susceptibility decreases, intravoxel dephasing decreases signal intensity (T2 or T2*) increases, and a local increase in image intensity on T2*-weighted images (5%).

Functional MRI techniques measure two basic physiological effects in areas of cortical activity: (1) an increase in blood flow/volume; and (2) a decrease in deoxyhemoglobin concentration in venous blood.

A decrease in dexoyhemoglobin concentration reduces magnetic susceptibility in venous blood and produces an increase in T2*, increasing the signal in T2*-weighted images.

Statistical techniques are used to calculate a fMRI image of the cortical region involved with the activation task. In the simplest treatment, control images are averaged and subtracted from an average activated image to produce a fMRI image.

A. Data processing

The fMRI datasets are processed to produce one fMRI image for each tomographic slice. As mentioned previously, the simplest approach to data analysis is to subtract the average image of the control state from the average image acquired of the activated state. For robust activation tasks such as motor activation, this can produce a fMRI image, demonstrating intensity along the central sulcus, with noisy background data elsewhere. The significance of such a result is uncertain since the number of activated voxels is straightforwardly affected by any numerical threshold applied or the window and level adjustment of the lookup table used to display the image.

The next level of sophistication in dataset analysis may reside on the MRI scanner. Some modern scanners incorporate some capability to perform a paired data *t* test or *Z* score on each slice on a voxel-by-voxel basis. The *Z* score is computed as

$$Z=\frac{\overline{X}_a-\overline{X}_c}{\sqrt{\frac{\Sigma(X_a-\overline{X}_a)^2}{N_a-1}+\frac{\Sigma(X_c-\overline{X}_c)^2}{N_c-1}}},$$

where X_a represents data from the activated state, X_c represents data from the control state, N_a represents the number of activated images, N_c represents the number of control images, and Z is a "*t*"-like statistic

Results of such calculations can be displayed on the scanner consoles and results can be archived as part of the patient data. Processing of fMRI datasets on the scanner can take as much as one hour of compute time, which may slow down the MRI scanner or make it unavailable for imaging.

Language and memory tasks produce activation that is more widely distributed and less robust than motor tasks. As a result, subtraction, *t*-test or *Z*-score approaches are generally inadequate. Several additional processing steps are often used in fMRI data analysis.

Many data processing approaches are based on cross-correlation. Voxel time courses undergo a cross-correlation with a boxcar function, or similar tailored function having the same period as the activation task. The boxcar reference curve has a value of zero when the patient is performing a control task and a value of 1 when the patient is performing an activation task. The cross-correlation analysis produces two results for each voxel. One result is the magnitude of signal change that occurs in synchrony with the activation task. The second result is the statistical significance of the magnitude observed (*p* value). In analyses that incorporate a delta time term in the model, the timing of the reference curve is adjusted or fitted for each voxel time course in order to account for the latency between cerebral activation and cerebrovascular response.

B. Controlling motion artifact

Gross physiologic motion, respiratory motion, and cardiac pulsation cause the brain to move throughout a fMRI study. Such motion can cause an artifact in fMRI results. Motion artifact often present as seemingly activated voxels along the periphery of the brain or along boundaries between dissimilar tissue (ventricles, sinuses). Essentially, motion may cause a spatial voxel located between dissimilar tissues to vacillate between the T2*-weighted intensities associated with the two tissues. If this vacillation has a time course somewhat similar to the time course of the activating task, the voxels can appear significant in the fMRI images. It is widely held that motion much smaller than the voxel dimensions can produce significant motion artifacts in fMRI results.

There are at least four approaches for controlling motion artifact.

One approach is to coregister each stack of tomographic slices to a selected stack. This typically involves a rigid body rotation of each dataset, and may or may not include temporal fitting or smoothing.

The second approach is to assume that rigid body rotations may create as many problems as they solve since the brain is in fact a deformable body. In this case, the approach becomes two pronged. First, eliminate motion by aggressive use of head fixation (padding or vacuum fixation bags), expandable foam, hammock, bite blocks, or a thermoplastic mesh mask. Second, carefully examine the datasets for evidence of motion and set aside any data demonstrating significant motion. Pressure sensors placed around the head can be used to monitor motion during the course of a fMRI study. Motion can be detected retrospectively by playing each tomographic slice in a CINE loop and visually observing movement between frames. In viewing a CINE loop, it may be helpful to subtract each tomographic slice from a selected tomographic slice, in which case the significant content of each subtracted image represents the motion associated with the slice. Alternatively, the coordinates of the center of mass of each dataset can be plotted for the time course of the study. Any acquisitions demonstrating motion should be set aside, and excluded from further analysis.

The third approach involves monitoring the physiological

processes that contribute to motion and subsequently removing contributions to each voxel time course that have the same waveform. The digitization of ECG data documents the waveform associated with cardiac pulsatility. The digitization of pneumatic pressure in a bellows or CO_2 concentration from a capnograph documents the waveform associated with respiration. The resultant digitized cardiac and respiratory waveforms can be used to process raw voxel time course data to correct for cardiac motion and respiratory motion.

In the fourth approach, voxel time course data can be analyzed using power spectral density techniques. Using power spectral density techniques, the variation in the data that occurs at the native frequency of the activating task is emphasized and the variation that occurs at the frequencies associated with the cardiac cycle or respiratory cycle is suppressed.

C. Accommodating hemodynamic latency

As introduced previously, there is a latency of approximately 5–9 s that occurs between the onset/cessation of activation and an increase/decrease in T2* contrast. When using simple subtraction for fMRI data analysis, you can attempt to control for this phenomenon by judiciously choosing which acquisitions are likely to represent activation and control. Since each patient and each region of cerebral cortex demonstrate different latency, this approach may not be adequate. A more sophisticated approach is to include a delta time term in the model used for data analysis of each voxel time course.

D. Accommodating baseline drift

It is not uncommon for the voxel time course to demonstrate a near linear baseline drift during the course of a study. The origin of this drift is not clearly understood. It is sometimes attributed to the heating of rf and gradient coils during an extended pulse sequence having high duty cycles. It is also attributed to determinate electronic errors that can be eliminated by aggressive maintenance of the MRI system. Nonetheless, linear baseline drifts can be incorporated in the model used for data analysis and effectively diminished.

E. Voxel clusters

In order to improve the selectivity of the fMRI technique and to minimize the contribution of individual artifactual voxels, a cluster criteria can be applied to the fMRI results. The effect of a cluster is to eliminate activated voxels that are not in a cluster having a significant volume.

F. Normalization of volume datasets

Finally, when looking for significant patterns of activation in a population of patients, it is convenient to map each patient's fMRI results into a normalized space. One popular approach is to map each patient's data into the Talairach–Tournoux coplanar stereotactic space. Statistical techniques (ANOVA, ANCOVA) can then be used to detect cortical areas having significant activation across subjects.

G. Data display

The intensity of each pixel in a fMRI image is often converted to a color using a color lookup table. The *p* values can be used for displaying only those voxels whose correlation exceeds a significance threshold. Each thresholded fMRI color image can then be overlaid on the associated native echoplanar T2*-weighted gray scale image or reformatted high resolution T1-weighted gray scale image.

H. fMRI artifacts

Artifacts in fMRI images include the patient motion described above (bulk motion, cardiac, respiratory). Nonrigid body movement of brain parenchyma caused by cardiac pulsations can produce artifacts as large as a few percent of BOLD contrast. These artifacts occur predominantly near CSF (brainstem, cerebellum). Bulk physiological motion causes voxels on the periphery of the brain to appear activated.

Additionally, geometric distortion due to B_o inhomogeneity produces significant artifacts in fMRI. Due to increased susceptibility effects, the EPI sequences used frequently in fMRI are particularly sensitive to B_o inhomogeneity. Magnetic field inhomogeneity can result from inhomogeneity of the magnet B_o field, as well as various susceptibilities of patients' tissues, particularly near the boundaries of tissues having disparate susceptibility (tissue/air, tissue/bone). The sphenoid sinus causes magnetic susceptibility artifacts in EPI images in the inferior frontal cortex and the inferior lateral temporal cortex. A transverse–oblique orientation could be tilted 10°–15° toward the coronal plane to maximize brain coverage, as well as reduce susceptibility artifacts near the base of the brain. Another source of susceptibility artifact is the movement of the chest during respiration. Although the chest is outside the field of view being imaged, phase changes of 2°–6° at an echo time of 40 ms can occur due to respiration. Likewise, movement of the arms and legs can induce fluctuations in magnetic susceptibility inside the sensitive volume of the rf coil.

The relatively late effective echo time (40–60 ms) used in many fMRI EPI pulse sequences can cause an artifact. The loss in signal due to T2* decay during the phase encoding of a single shot image produces a modulation of the raw *k*-space data, which transforms to blurring of the reconstructed EPI images.

I. fMRI data analysis software

There are several substantial software packages dedicated to processing functional datasets. These software packages incorporate many of the features described above with respect to motion detection and correction, fitting of temporal latency, and normalization to a standard feature space.

A package useful for detection of motion artifact and rigid body correction of motion in tomographic datasets is the following.

Automated Image Registration (AIR). Roger Woods,[80–82] UCLA, http://bishopw.loni.ucla.edu.

Major packages for processing of fMRI datasets include the following.

(i) **Analysis of Functional Neurological Images (AFNI):** Robert Cox, Medical College of Wisconsin, http://afni.nimh.nih.gov/afni.
Features: *t* tests; cross-correlation to a user-defined stimulation reference curve; shift the reference curve in time to find the optimum temporal; registration between the voxel time course and the stimulation reference curve; image registration to correct for rigid body motion; baseline correction of any constant offset or slope (or higher order) in the time course data for a voxel; multiplanar reformats; graphs of voxel time course; ANOVA tests for comparing patient populations; C source code is distributed freely; can be run via Graphical User Interface or via command line.

(ii) STIMULATE: John Strupp,[83–87] Center for Magnetic Resonance Research, University of Minnesota, http://www.cmrr.drad.umn.edu/stimulate/.Features: similar to AFNI, but with fewer post-processing test options; does not include rigid body image reregistration to correct for rigid motion; compiled binary distribution; can start from raw *k*-space data; will report the latency of cerebral activation; can be run via the Graphical User Interface.

(iii) **Statistical Parametric Mapping (SPM):** Karl Friston,[88–98] Welcome Department of Cognitive Neurology, Institute of Neurology, University College of London, http://www.fil.ion.ucl.ac.uk/spm/.

Sensor Systems and NIH are porting SPM to C++ libraries for use via MEDx (medical image analysis and visualization software).

Features: suite of MatLab functions and routines; a very powerful statistical package offering parametric statistical models using the general linear model to describe the variability in the data in terms of experimental and confounding effects and residual variability; incorporates statistical analysis of spatial extent of activation clusters; incorporates segmentation of white matter, gray matter, and CSF; incorporates volume rendering of fMRI results on fixed views of a standard brain.

APPENDIX: PROTOCOLS FOR VARIOUS ACTIVATION TASKS

A. Institution: University of Texas Southwestern Medical Center at Dallas
Contact person: Roddy McColl
fMRI description: Multi-slice GE-EPI
Title/purpose: To elicit working memory deficit in brain-injured adolescents
Pulse sequence description:

Pulse seq	FOV (mm)	Matrix size	Slice (mm)	TR/TE	Baseline epoch (s)	Activation epoch (s)	Base/Act cycles	Total images	Total time (min:s)
GE(90°)	340	96×96	3.8	4000/40	24	24	16	2304	12:48

Anatomical position information: Axial slices to cover cerebrum
Statistical treatment method: Correlation analysis (Bandettini)[99]

Task description:

1. Presents single letters every 2 seconds—was this letter seen two letters back?
2. Presents two letter groups every 2 seconds—is the letter the same?

B. Institution: University of Texas Southwestern Medical Center at Dallas
Contact person: Roddy McColl
fMRI description: Multi-slice GE-EPI for working memory
Title/purpose: To elicit working memory centers in elderly subjects

Pulse sequence description:

Pulse seq	FOV (mm)	Matrix size	Slice (mm)	TR/TE	Baseline epoch (s)	Activation epoch (s)	Base/Act cycles	Total images	Total time (min:s)
GE(90°)	340	96×96	3.8–7.0	4000/40	16	16	32	4096–7168	17:00

Anatomical position information: Axial slices to cover entire cerebrum
Statistical treatment method: Correlation analysis (Bandettini)[99]

Task description:

1. Grid is presented with consonants in some cells of the grid
2. An empty grid replaces original
3. A single letter is placed on grid
4a. Was this letter on before
4b. Was this cell filled

C. Institution: University of Texas Southwestern Mecial Center at Dallas
Contact person: Roddy McColl
fMRI description: Multi-slice GE-EPI
Title/purpose: Ongoing fMRI development using motor tasks

Pulse sequence description:

Pulse seq	FOV (mm)	Matrix size	Slice (mm)	TR/TE	Baseline epoch (s)	Activation epoch (s)	Base/Act cycles	Total images	Total Time (min:s)
GE(90°)	340	96×96	3.5–5.0	4000/40	⩾16	⩾16	⩾4	360–1080	3:00–6:40

Anatomical position information: Axial slices to cover motor strip
Statistical treatment method: Correlation analysis (Bandettini)[99]

Task description:

1. Subject alternates between rest and bilateral hand clenching

D. Institution: Medical College of Georgia
Contact person: Jerry Allison
fMRI description: Motor task activation: Language tasks
Title/purpose: Language lateralization: Motor strip localization

Pulse sequence description:

Pulse seq	FOV (mm)	Matrix size	Slice (mm)	TR/TE	Baseline epoch (s)	Activation epoch (s)	Base/Act cycles	Total images	Total time (min:s)
GE(90°)	172×230	64×128	6.0	3000/64	30	30	6	2048	6:24

Anatomical position information: Whole brain/head coil/transverse obliques (T→C, −20°)
Statistical treatment method: Statistical parametric mapping (SPM)

Task description:

1. Verb generation task: Alternation between visual presentation of short nouns and simple plus signs. The patient silently generates a verb when they see a noun. Keypad response is used to assure attentiveness.
2. Exercise task: Alternation between resting, left-hand finger tapping and right-hand finger tapping. Shown below is activation of the left motor strip and right cerebellum associated with right-hand finger tapping. Note that the right hemisphere is on the right side of the SPM ''glass'' brain presentation (Fig. 2).

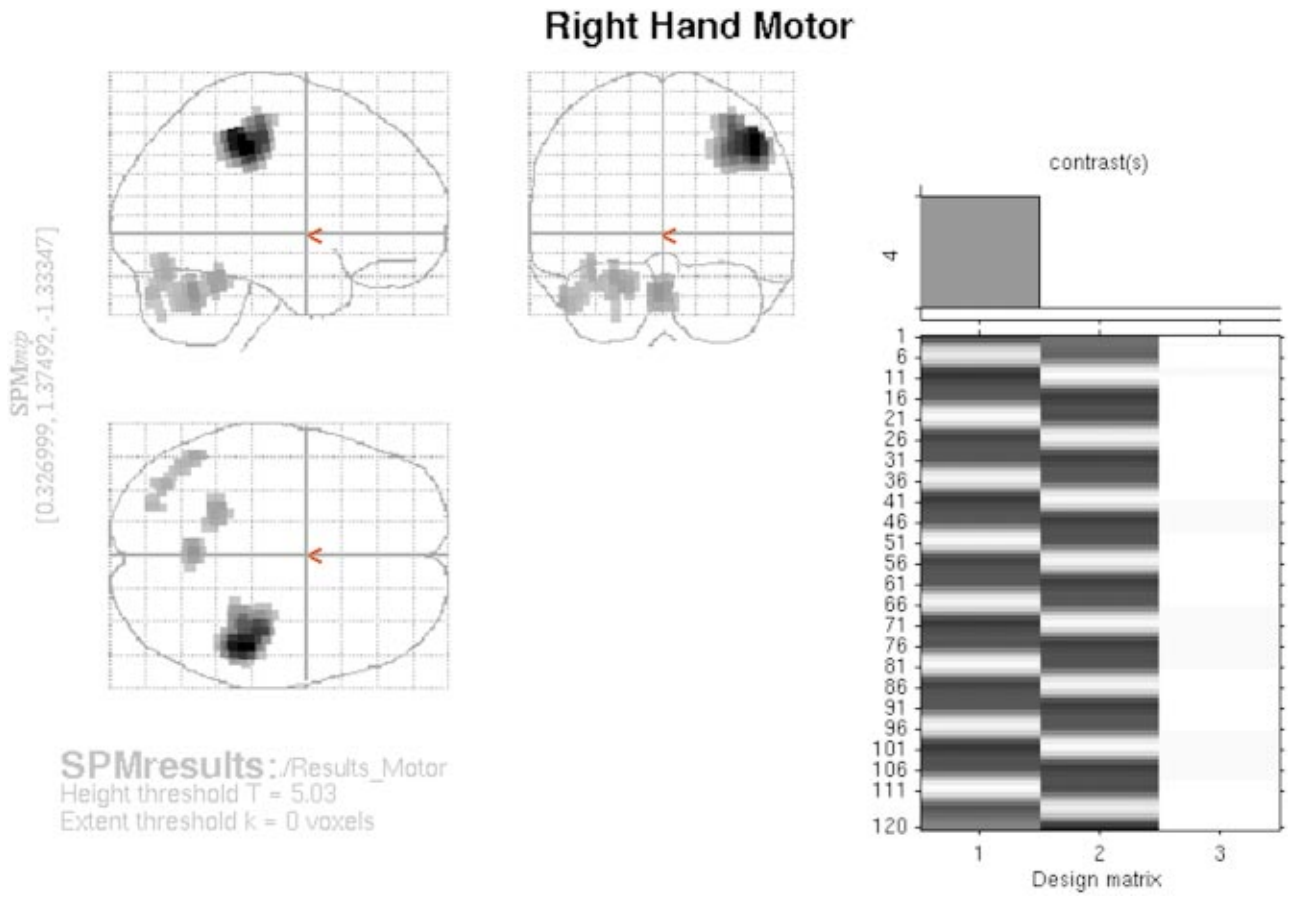

FIG. 2. Typical fMRI output of the SPM software package in which the ''glass'' brain presents orthogonal projection images of all ''activated'' voxels.

E. Institution: Vanderbilt University
Contact person: Ronald R. Price
fMRI description: Cerebellar activation—Fine motor function
Title/purpose: Recovering alcoholics
Pulse sequence Description:

Pulse seq	FOV (mm)	Matrix size	Slice (mm)	TR/TE	Baseline epoch (s)	Activation epoch (s)	Base/Act cycles	Total images	Total time (min:s)
GE(90°)	240	64×64	5.0	4000/60	40	40	8	960	10:40

Anatomical position information: Head coil/Cerebellum
Statistical treatment method: *t* test or cross-correlation

Task description:

1. Computer monitored finger tapping of index finger (40 s tapping, 40 rest cycles)
2. Repeat study for dominant/nondominant hand.
3. fMRI output from the STIMULATE (http://www.cmrr.drad.umn.edu/stimulate/) fMRI software package (Fig. 3).

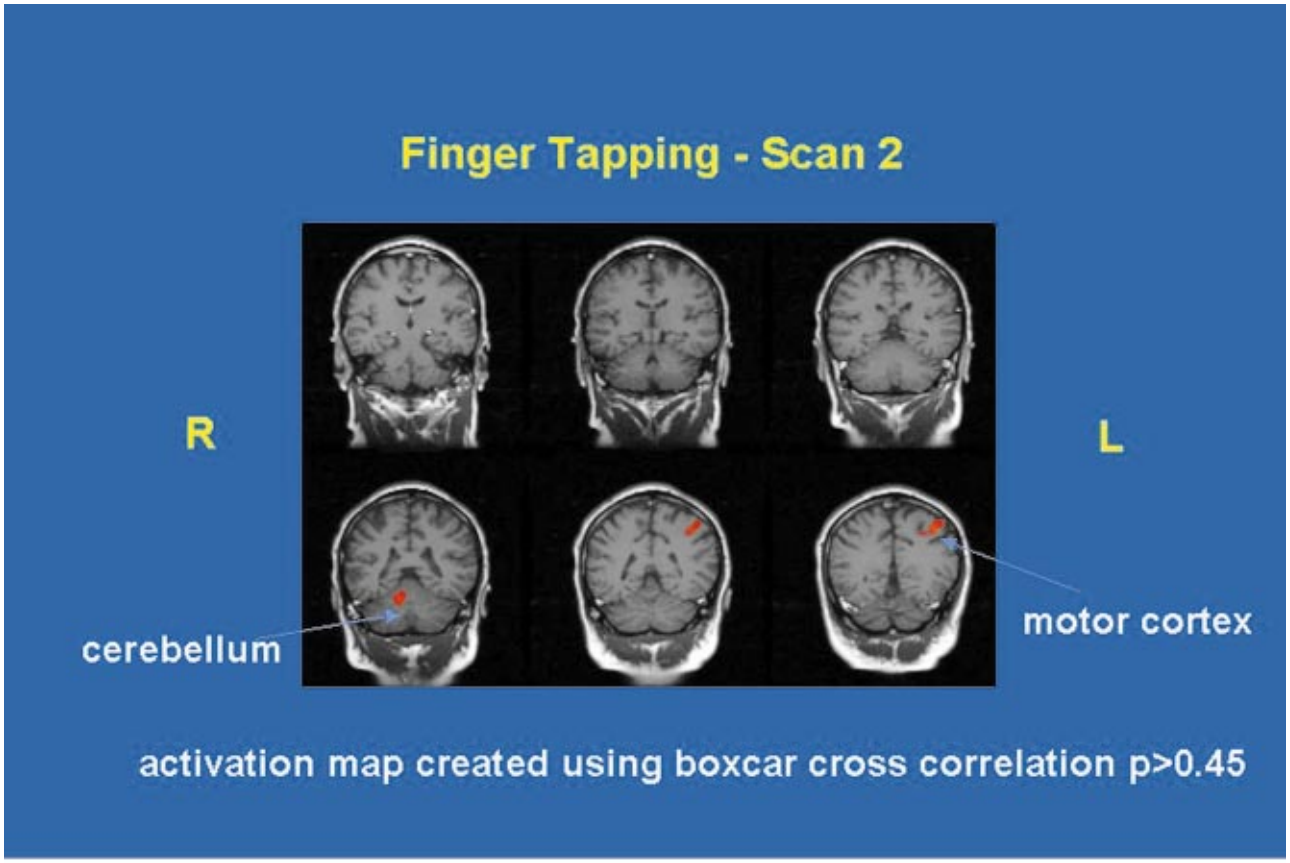

(a)

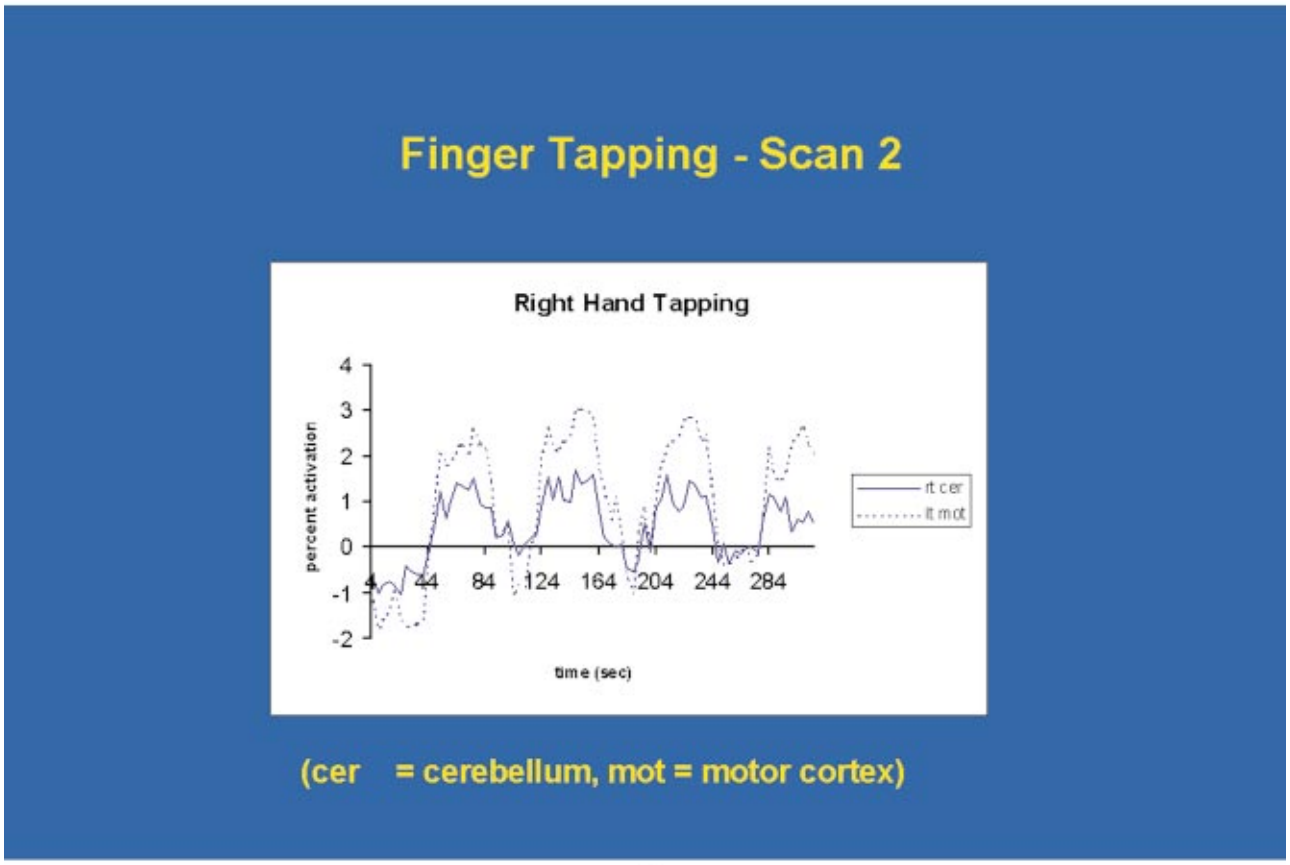

(b)

FIG. 3. (a) Color overlay of activated voxels over high-resolution anatomical images. (b) Time-intensity plot of activated regions from a ''block-mode'' task showing four activation epochs and four rest epochs.

F. Institution: Medical College of Wisconsin
Contact person: F. Yetkin
fMRI description: Motor task activation
Title/purpose: Retest accuracy

Pulse sequence description:

Pulse seq	FOV (mm)	Matrix size	Slice (mm)	TR/TE	Baseline epoch (s)	Activation epoch (s)	Base/Act cycles	Total images	Total time (min:s)
GE(90°)	240	64×64	10	1000/40	20	20	4/3	140	2:33

Anatomical position information: Head coil
Statistical treatment method: Cross-correlation

Task description:

1. Touching thumb to index finger

G. Institution: Mass General Hospital
Contact person: Roger Tootell
fMRI description: fMRI of visual motion, color and luminance
Title/purpose: fMRI of Human MT and Related Visual Cortex

Pulse sequence description:

Pulse seq	FOV (mm)	Matrix size	Slice (mm)	TR/TE	Baseline epoch (s)	Activation epoch (s)	Base/Act cycles	Total images	Total time (min:s)
GE(90°)	400	128×128	6	2000/50	40	40	6	720	8:00

Anatomical position information: 5 in. surface coil—Lateral to occipital pole
Statistical treatment method: Komolgorov–Smimov analyses of stimulus-locked activity

Task description:

1. Rear projection video
2. Alternating image with blank screen
3. Stimuli of equal length 30–45 s

H. Institution: Mass General Hospital
Contact person: Roger Tootell
fMRI description: Occipital cortex
Title/purpose: Object related activation

Pulse sequence description:

Pulse seq	FOV (mm)	Matrix size	Slice (mm)	TR/TE	Baseline epoch (s)	Activation epoch (s)	Base/Act cycles	Total images	Total time (min:s)
GE(90°)	400	64×128	6	3000/80	30	30	6	960–1020	4:00–9:00

Anatomical position information: 5 in. surface coil placed posterolaterally
Statistical treatment method: Voxel-by-voxel Komolgorov–Smimov statistic

Task description:

1. Visual stimuli (5–12 scans)
2. 960–1020 images over 240–540 s
3. 11–12 epochs alternate pictures with blank screen

I. Institution: Vanderbilt University
Contact person: Ronald R. Price
fMRI description: Brain mapping during Braile reading
Title/purpose: Brain organization in blind individuals as a function of the onset of blindness

Pulse sequence description:

Pulse seq	FOV (mm)	Matrix size	Slice (mm)	TR/TE	Baseline epoch (s)	Activation epoch (s)	Base/Act cycles	Total images	Total time (min:s)
GE(90°)	240	64×64	5.0	4000/60	40	40	8	960	10:40

Anatomical position information: Oblique slices/head coil over visual cortex with additional slices over sensory/motor strip
Statistical treatment method: *t* test or cross-correlation

Task description:

1. Subject reads Braille for 40 s followed by 40 s rest
2. Subject's fingers are brushed for periods of 40 s to identify the sensory area
3. Subjects given panel of small objects to identify
4. STIMULATE (Ref. 84) fMRI output, Fig. 4.

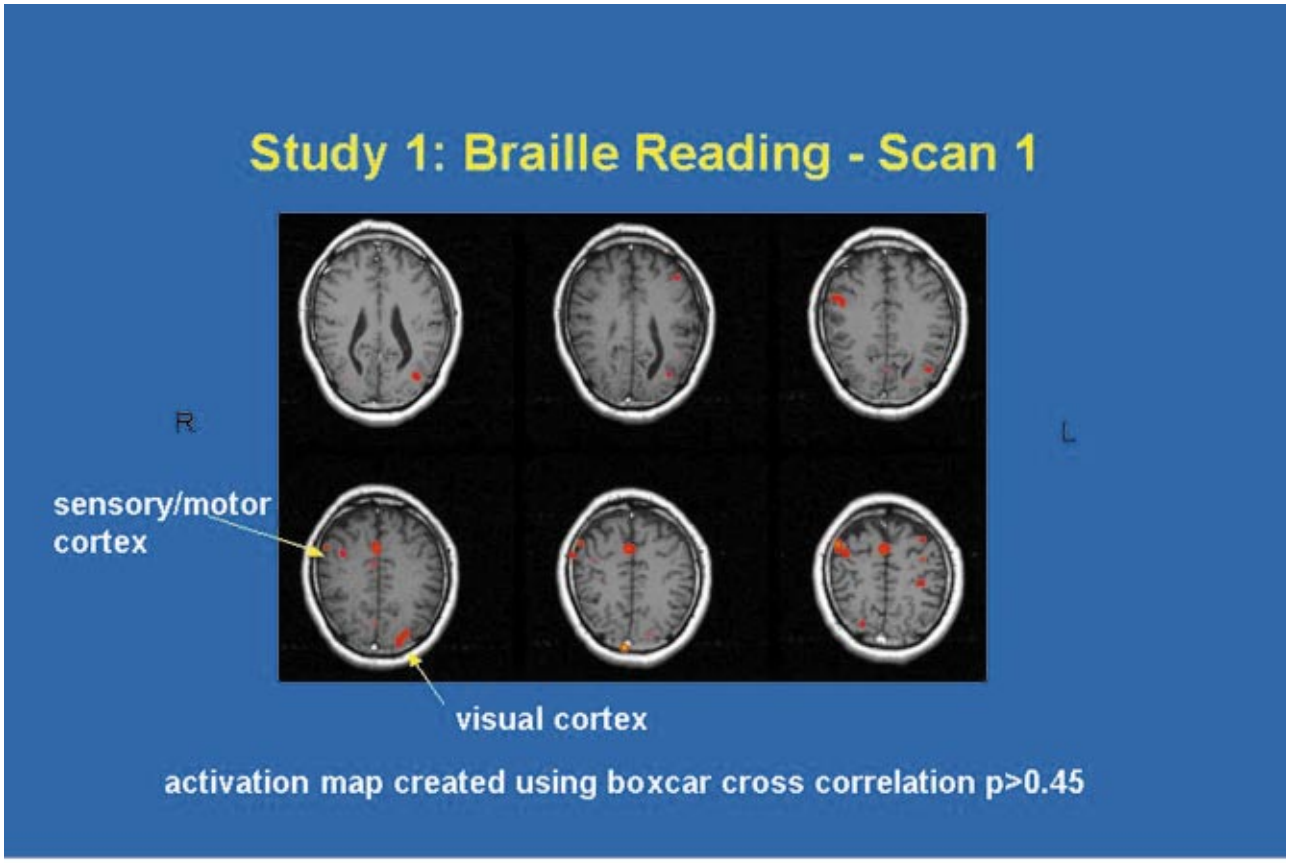

(a)

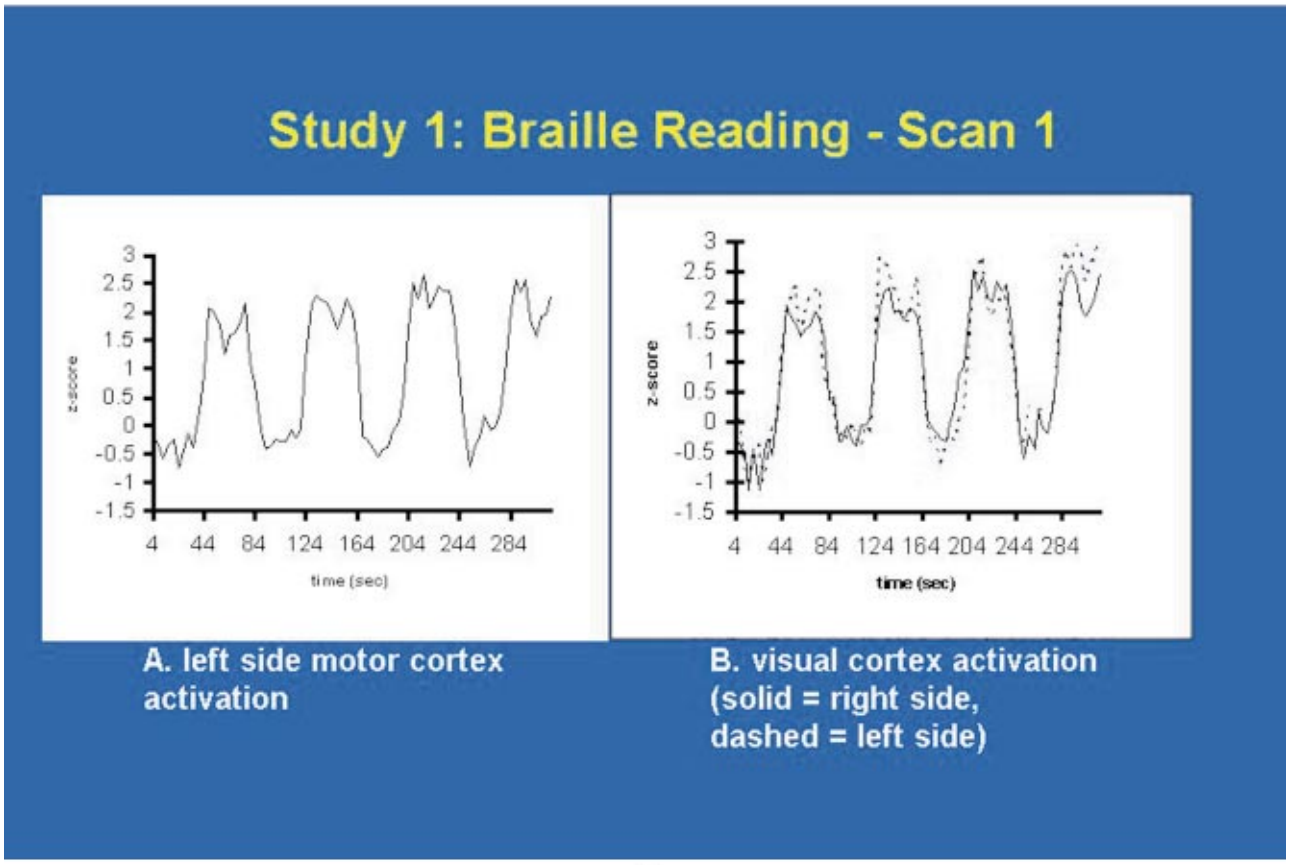

(b)

FIG. 4. (a) Color overlay of activated voxels. (b) Time-intensity plots of activated regions over the motor cortex and the visual cortex.

[a]Corresponding address: Ronald R. Price, Ph.D., Department of Radiology, Vanderbilt University Medical Center, 1161 21st Avenue South, Nashville, Tennessee 37232-2675. Telephone: (615)322-3190; Fax: (615) 322-3874; electronic mail: ron.price@mcmail.vanderbilt.edu

[1] P. C. Lauterbur, ''Image formation by induced local interactions: Examples employing nuclear magnetic resonance,'' Nature (London) **242**, 190–191 (1973).
[2] S. Ogawa *et al.*, ''Oxygenation-sensitive contrast in magnetic resonance imaging of rodent brain at high magnetic fields,'' Magn. Reson. Med. **14**, 68–78 (1990).
[3] K. R. Thulborn *et al.*, ''Oxygenation dependence of the transverse relaxation time of water protons in whole blood at high field,'' Biochim. Biophys. Acta **714**, 265–270 (1982).
[4] R. A. Brooks and G. DiChiro, ''Magnetic resonance imaging of stationary blood: A review,'' Med. Phys. **14**, 903–913 (1987).
[5] S. Ogawa and T. Lee, ''Magnetic resonance imaging of blood vessels at high fields: In vivo and in vitro measurements and image simulation,'' Magn. Reson. Med. **6**, 9–18 (1990).
[6] R. Turner *et al.*, ''Echo-planar time course MRI of cat brain oxygenation changes,'' Magn. Reson. Med. **22**, 159–166 (1991).
[7] S. Ogawa, T. M. Lee, and B. Barrere, ''The sensitivity of magnetic resonance image signals of a rat brain to changes in the cerebral venous blood oxygenation,'' Magn. Reson. Med. **29**, 205–210 (1993).
[8] K. K. Kwong *et al.*, ''Dynamic magnetic resonance imaging of human brain activity during primary sensory stimulation,'' Proc. Natl. Acad. Sci. U.S.A. **89**, 5675–5679 (1992).
[9] P. T. Fox *et al.*, ''Mapping the human visual cortex with positron emission tomography,'' Nature (London) **323**, 806–809 (1986).
[10] P. T. Fox *et al.*, ''Focal physiological uncoupling of cerebral blood flow and oxidative metabolism during somatosensory stimulation in human subjects,'' Neurobiology **83**, 1140–1144 (1986).
[11] J. W. Belliveau *et al.*, ''Functional mapping of the human visual cortex by MRI,'' Science **254**, 716–719 (1991).
[12] P. T. Fox *et al.*, ''Nonoxidative glucose consumption during focal physiologic neural activity,'' Science **241**, 462–464 (1988).
[13] R. D. Frostig *et al.*, ''Cortical functional architecture and local coupling between neuronal activity and the microcirculation revealed by in vivo high resolution optical imaging of intrinsic signals,'' Proc. Natl. Acad. Sci. U.S.A. **15**, 6082–6086 (1990).
[14] J. W. Belliveau *et al.*, ''Functional cerebral imaging by susceptibility-contrast NMR,'' Magn. Reson. Med. **14**, 538–546 (1990).
[15] B. R. Rosen *et al.*, ''Susceptibility contrast imaging of cerebral blood volume: Human experience,'' Magn. Reson. Med. **22**, 293–299 (1991).
[16] R. M. Weisskopf and S. Kiihne, ''MRI susceptometry: Image-based measurement of absolute susceptibility of MR contrast agents and human blood,'' Magn. Reson. Med. **24**, 375–383 (1992).
[17] S. Ogawa *et al.*, ''Brain magnetic resonance imaging with contrast dependent on blood oxygenation,'' Proc. Natl. Acad. Sci. U.S.A. **87**, 9868–9872 (1990).
[18] S. Ogawa *et al.*, ''Functional brain mapping by blood oxygenation level-dependent contrast MRI,'' Biophys. J. **64**, 803–812 (1993).
[19] R. Turner *et al.*, ''Functional mapping of the human visual cortex at 4 and 1.5 Tesla using deoxygenation contrast EPI,'' Magn. Reson. Med. **29**, 277–279 (1993).
[20] G. A. Wright, B. S. Hu, and A. Macovski, ''Estimating oxygen saturation of blood in vivo with MRI at 1.5 T,'' J. Magn. Reson Imaging **1**, 275–283 (1991).
[21] J. M. Gomori *et al.*, ''NMR relaxation times of blood: Dependence on field strength, oxidation state, and cell integrity,'' J. Comput. Assist. Tomogr. **11**, 684–690 (1987).
[22] R. C. Fisel *et al.*, ''MR contrast due to microscopically heterogeneous magnetic susceptibility: Numerical simulations and applications to cerebral physiology,'' Magn. Reson. Med. **17**, 336–347 (1991).
[23] P. Jezzard *et al.*, ''An investigation of the contribution of physiological noise in human functional MRI studies at 1.5 Tesla and 4 Tesla,'' *Proceedings of the 12th SMRM Annual Meeting*, New York, 1993, 1392.
[24] P. A. Bandettini *et al.*, ''Time course EPI of human brain function during task activation,'' Magn. Reson. Med. **25**, 390–397 (1992).
[25] J. Frahm *et al.*, J. Magn. Reson Imaging **2**, 501 (1992).
[26] S. Ogawa *et al.*, ''Intrinsic signal changes accompanying sensory stimulation: Functional brain mapping with MRI,'' Proc. Natl. Acad. Sci. U.S.A. **89**, 5951–5955 (1992).
[27] R. S. Menon *et al.*, ''Functional brain mapping using MRI: Signal changes accompanying visual stimulation,'' Invest Radiol. **27**, S47–53 (1992).
[28] E. A. DeYoe *et al.*, ''Time course of event-related MR signal enhancement in visual and motor cortex,'' *Proceedings of the 11th SMRM Annual Meeting*, Berlin, 1992, p. 1824.
[29] A. M. Blamire *et al.*, ''Dynamic mapping of the human visual cortex by high-speed MRI,'' Proc. Natl. Acad. Sci. U.S.A. **89**, 11 069–11 073 (1992).
[30] R. L. Grubb *et al.*, ''The effects of changes in PaCO2 on cerebral blood volume, blood flow and vascular mean transit time,'' Stroke **5**, 630–639 (1974).
[31] D. Bereczki *et al.*, ''Hypoxia increases velocity of blood flow through parenchymal microvascular systems in rat brain,'' J. Cereb. Blood Flow Metab. **11**, S72 (1993).
[32] R. Turner, P. Jezzard, and F. Heineman, ''Quantitative studies of EPI BOLD contrast with animal models,'' *Syllabus of the SMRM fMRI Workshop*, Arlington, VA, 1993, pp. 121–128.
[33] S. G. Kim *et al.*, ''Functional imaging of human motor cortex at high magnetic field,'' J. Neurophysiol. **69**, 297–302 (1993).
[34] S. M. Rao *et al.*, ''Functional MRI of complex human movements,'' Neurology **43**, 2311–2318 (1993).
[35] P. A. Bandettini *et al.*, ''Spin-echo and gradient-echo EPI of human brain activation using BOLD contrast: A comparative study at 1.5 T,'' NMR Biomed. **7**, 12–20 (1994).
[36] J. L. Boxerman *et al.*, ''The intravascular contribution to fMRI signal change: Monte Carlo modeling and diffusion-weighted studies in vivo,'' Magn. Reson. Med. **34**, 4–10 (1994).
[37] J. H. Duyn *et al.*, ''Inflow versus deoxyhemoglobin effects in 'BOLD' functional MRI using gradient echoes at 1.5 T,'' NMR Biomed. **7**, 83–88 (1994).
[38] S. Gromiscek *et al.*, ''A possible role of in-flow effects in functional MR imaging,'' Magn. Reson. Mater. Phys., Biol., Med. **1**, 109–113 (1993).
[39] S. Lai *et al.*, ''Identification of vascular structures as a major source of signal contrast in high resolution 2D and 3D functional activation imaging of motor cortex at 1.5 T: Preliminary results,'' Magn. Reson. Med. **30**, 387–392 (1993).
[40] S. G. Kim *et al.*, ''Potential pitfalls of functional MRI using conventional gradient-recalled echo techniques,'' NMR Biomed. **7**, 69–74 (1994).
[41] A. T. Lee, G. H. Glover, and C. H. Meyer, ''Discrimination of large venous vessels in time-course spiral blood-oxygen-level-dependent magnetic-resonance functional neuro-imaging,'' Magn. Reson. Med. **33**, 745–754 (1995).
[42] J. W. Belliveau *et al.*, ''Functional mapping of the human visual cortex by magnetic resonance imaging,'' Science **254**, 716–719 (1991).
[43] M. I. Sereno *et al.*, ''Borders of multiple visual areas in humans revealed by functional magnetic resonance imaging,'' Science **268**, 889–893 (1995).
[44] A. G. Sorensen, *et al.*, ''Extrastriate activation in patients with visual field defects,'' in Ref. 23, p. 62.
[45] C. R. Jack, Jr. *et al.*, ''Sensory motor cortex: Correlation of presurgical mapping with functional MR imaging and invasive cortical mapping,'' Radiology **190**, 85–92 (1994).
[46] J. K. Hirsch, K. Kim, K. Lee, G. Krol, and M. Souweidane. A four-part battery of fMRI tasks for neurosurgical planning, *Proceedings of the ISMRM 5th Annual Meeting*, 1997, p. 694.
[47] J. C. Lin, J. R. Gates, F. J. Ritter, M. B. Dunn, X. Hu, T. Kato, C. A. Nelson, and C. L. Truwit, preoperative functional MR imaging to assess language and memory lateralization in patients with surgical brain disease, in Ref. 46, p. 693.
[48] C. Tegeler, B. Gaschler, F. Baumgart, C. Tempdmann, D. Stiller, F. Schindler, H. Heinze, and H. Scheich, ''Temporal behavior of a particular human auditory cortex field activated by masked stimuli,'' in Ref. 46, p. 708.
[49] M. G. Woldorff, C. Tempelmann, C. Tegeler, B. Gaschler, H. Henrichs, H. Heinze, and H. Scheich, Lateralized auditory spatial perception and contra-laterality of cortical processing as studied with fMRI, in Ref. 46, p. 709.
[50] A. J. Freeman, C. M. Mohr, W. M. King, R. W. Briggs, and C. M. Leonard, ''Effect of stimulus intensity on the volume of activated cortex in auditory fMRI,'' in Ref. 46, p. 710.
[51] K. Kuppusamy, B. Lee, D. Elghazzawy, R. Grueneich, R. Gordon, W. Lin, and M. Haach, ''Pediatric fMRI study on hemispheric language dominance,'' in Ref. 46, p. 517.

[52] J. B. Dembo, J. E. Desmond, A. D. Wagner, C. J. Vaidya, G. H. Glover, and J. D. Gabrieti, ''Semantic encoding and retrieval in the left inferior prefrontal cortex: a functional MRI study of task difficulty and process specificity,'' J. Neurosci. **15**, 5870–5878 (1995).
[53] M. D'Esposito, B. R. Postle, J. Jonides, and E. E. Smith, ''The neural substrate and temporal dynamics of interference effects in working memory as revealed by event-related functional MRI,'' Proc. Natl. Acad. Sci. USA **96**, 7514–7519 (1999).
[54] S. L. Cramer, G. Nells, R. R. Benson, J. D. Kaplan, R. A. Parker, K. K. Kwong, S. P. Finkelstein, and B. R. Rosen, A functional MRI study of three motor tasks in the evaluation of recovery from stroke, in Ref. 46, p. 512.
[55] E. M. Vikingstad, Y. Cao, K. P. George, J. Faull, A. Johnson, and K. Welch, ''Using BOLD functional MRI to examine language systems in recovered aphasic stroke patients,'' in Ref. 46, p. 513.
[56] T. Yoshiura, K. Hasuo, F. Mihara, K. Masuda, T. Morioka, and M. Fujiu, ''Reorganization of motor cortex in patients with brain tumor,'' in Ref. 46, p. 514.
[57] L. Maccotta, J. A. Detre, D. C. Alsop, M. D'Esposito, L. R. Vives and E. C. Raps, ''fMRI patterns of motor activation in patients with cerebrovascular disease,'' in Ref. 46, p. 518.
[58] G. Liu, G. Sobering, A. W. Olson, P. van Gelderen, and C. T. W. Moonen, ''Fast echo-shifted gradient-recalled MRI: combining a short repetition time with variable T2* weighting,'' Magn. Reson. Med. **30**, 68–75 (1993).
[59] X. Hu and S-G. Kim, ''A new T2*-weighting technique for magnetic resonance imaging,'' Magn. Reson. Med. **30**, 512–517 (1993).
[60] R. T. Constable, R. P. Kennan, A. Puce, G. McCarthy, and J. C. Gore, ''Functional NMR imaging using fast spin echo at 1.5 T,'' Magn. Reson. Med. **31**, 686–690 (1994).
[61] J-H Rao, J. Xiong, J. Li, J. Schiff, J. Roby, J. L. Lancaster, and P. T. Fox, ''Fast spin echo characteristics of visual stimulation-induced signal changes in the human brain,'' J. Magn. Reson Imaging **5**, 709–714 (1995).
[62] M. K. Stehling, F. S. Schmitt, and R. Ladebeck, ''Echo-planar MR imaging of human brain oxygenation changes,'' J. Magn. Reson Imaging **3**, 471–474 (1993).
[63] P. A. Bandettini, E. C. Wong, R. S. Hinks, R. S. Tikofsky, and J. S. Hyde, ''Time course EPI of human brain function during task activation,'' Magn. Reson. Med. **25**, 390–397 (1992).
[64] J. Hirsch, R. L. DeLaPaz, N. R. Relkin, J. Victor, K. Kim, T. Li, P. Borden, N. Rubin, and R. Shapley, ''Illusory contours activate specific regions in human visual cortex: evidence from functional magnetic resonance imaging,'' Proc. Natl. Acad. Sci. U.S.A. **92**, 6469–6473 (1995).
[65] R. W. Cox, A. Jesmanowicz, and J. S. Hyde, ''Real-time functional magnetic resonance imaging,'' Magn. Reson. Med. **33**, 230–236 (1995).
[66] R. R. Edelman *et al.*, ''Qualitative mapping of cerebral blood flow and functional localization with echo-planar MR imaging and signal targeting with alternating radio frequency,'' Radiology **192**, 513–520 (1994).
[67] S-G. Kim, ''Quantification of relative cerebral blood flow change by flow sensitive alternating inversion recovery (FAIR) technique: application to functional mapping,'' Magn. Reson. Med. **34**, 293–301 (1995).
[68] J. A. Detre, J. S. Leigh, D. S. Williams, and A. P. Koretsky, ''Perfusion imaging,'' Magn. Reson. Med. **23**, 37–45 (1992).
[69] E. L. Barbier, A. C. Silva, S. G. Kim, and A. P. Koretsky, ''Perfusion imaging using dynamic arterial spin labeling (DASL),'' Magn. Reson. Med. **45**, 1021–1029 (2001).
[70] D. LeBihan, in *Diffusion and Perfusion Magnetic Resonance Imaging* (Raven, New York, 1995).
[71] K. J. Friston, *Image Processing of Functional MRI Data in Methods in Biomedical Magnetic Resonance Imaging and Spectroscopy*, edited by R. Young (Wiley, New York, 2000), Vol. 1, 585–602.
[72] K. Urgurbil, W. Chen, X. Hu, S. G. Kim, S. Ogawa, and X. H. Zhu, *Functional MRI at High Fields: Practice and Utility in Methods in Biomedical. Magnetic Resonance Imaging and Spectroscopy*, edited by I. R. Young (Wiley, New York, 2000), Vol. 1, pp. 603–622.
[73] P. A. Bandettini, J. R. Binder, E. DeYoe, and J. S. Hyde, *Hemodynamic Changes Owing to Sensory Activation of the Brain Monitored by Echo-Planar Imaging*, edited by I. R. Young (Wiley, New York, 2000), Vol. 1, pp. 623–630.
[74] K. K. Kwong, ''Functional magnetic resonance imaging with echo planar imaging,'' Magn. Reson. Q. **11**, 1–20 (1995).
[75] D. C. Noll, J. D. Cohen, C. H. Meyer, and W. Schneider, ''Spiral *k*-space MR imaging of cortical activation,'' J. Magn. Reson Imaging **5**, 49–56 (1995).
[76] G. H. Glover and A. T. Lee, ''Motion artifacts in fMRI: comparison of 2DFT with PR and spiral scan methods,'' Magn. Reson. Med. **33**, 612–635 (1995).
[77] X. Hu and S-G. Kim, ''Reduction of signal fluctuation in functional MRI using navigator echoes,'' Magn. Reson. Med. **31**, 495–503 (1994).
[78] S-G. Kim, X. Hu, G. Adriany, and K. Ugurbil, ''Fast interleaved echo-planar imaging with navigator: high resolution anatomical and functional images at 4 T,'' Magn. Reson. Med. **35**, 895–902 (1996).
[79] J-H. Gao, J. Xiong, S. Lai, E. M. Haacke, M. G. Woldorff, J. Li, and P. T. Fox, ''Improving the temporal resolution of functional MR imaging using keyhole techniques,'' Magn. Reson. Med. **35**, 854–860 (1996).
[80] J. Tailairach and P. Tournoux, *A Stereotactic Coplanar Atlas of the Human Brain* (Thieme, Stuttgart, 1988).
[81] R. P. Woods, S. R. Cherry, and J. C. Mazziotta, ''Rapid automated algorithm for aligning and reslicing PET images,'' J. Comput. Assist. Tomogr. **16**, 620–633 (1992).
[82] R. P. Woods, J. C. Mazziotta, and S. R. Cherry, ''MRI-PET registration with automated algorithm,'' J. Comput. Assist. Tomogr. **17**, 536–546 (1993).
[83] S. Ogawa *et al.*, ''Intrinsic signal changes accompanying sensory stimulation: functional brain mapping with magnetic resonance imaging,'' Proc. Natl. Acad. Sci. U.S.A. **89**, 5951–5955 (1992).
[84] K. J. Friston, ''Bayesian estimation of dynamical systems: An application to FMRI,'' Neuroimage **16**, 513–530 (2002).
[85] M. Press, B. Flannery, S. Teukolsky, and M. Vetterling, *Numerical Recipes in C* (Cambridge University Press, Cambridge, 1991).
[86] S. Kim, K. Hendrich, X. Hu, H. Merkle, and K. Ugurbil, ''Potential pitfalls of functional MRI using conventional gradient-recalled echo techniques,'' NMR Biomed. **7**, 69–74 (1994).
[87] S. Ogawa, D. Tank, R. Menon, J. Ellerman, S. Kim, H. Merkle, and K. Ugurbil, ''Intrinsic signal changes accompanying sensory stimulation: Functional brain mapping with magnetic resonance imaging,'' Proc. Natl. Acad. Sci. U.S.A. **89**, 5951–5955 (1992).
[88] K. J. Friston, K. J. Worsley, R. S. J. Frackowiak, J. C. Mazziotta, and A. C. Evans, ''Assessing the significance of focal activations using their spatial extent,'' Hum. Brain Mapp **1**, 214–220 (1994).
[89] K. J. Friston, P. Jezzard, and R. Turner, ''Analysis of functional MRI time-series,'' Hum. Brain Mapp **1**, 153–171 (1994).
[90] K. J. Friston, J. Ashburner, J. B. Poline, C. D. Frith, J. D. Heather, and R. S. J. Frackowiak, ''Spatial registration and normalization of images,'' Hum. Brain Mapp **2**, 165–189 (1995).
[91] K. J. Friston, A. P. Holmes, K. J. Worsley, J. P. Poline, C. D. Frith, and R. S. J. Frackowiak, ''Statistical parametric maps in functional imaging: A general linear approach,'' Hum. Brain Mapp **2**, 189–210 (1995).
[92] K. J. Friston, A. Holmes, J. B. Poline, C. J. Price, and C. D. Frith, ''Detecting activations in PET and fMRI: Levels of inference and power,'' Neuroimage **4**, 223–235 (1995).
[93] K. J. Friston, A. P. Holmes, J. B. Poline, P. J. Grasby, S. C. R. Williams, R. S. J. Frackowiak, and R. Turner, ''Analysis of fMRI time series revisited,'' Neuroimage **2**, 45–53 (1995).
[94] K. J. Friston, C. D. Frith, R. Turner, and R. S. J. Frackowiak, ''Characterizing evoked hemodynamics with fMRI,'' Neuroimage **2**, 157–165 (1995).
[95] K. J. Friston, C. D. Frith, R. S. J. Frackowiak, and R. Turner, ''Characterizing dynamic brain responses with fMRI: A multivariate approach,'' Neuroimage **2**, 166–172 (1995).
[96] K. J. Friston, S. R. Williams, R. Howard, R. S. J. Frackowiak, and R. Turner, ''Movement-related effects in fMRI time-series,'' Magn. Reson. Med. **35**, 346–355 (1996).
[97] K. J. Worsley and K. J. Friston, ''Analysis of fMRI time-series revisited—Again,'' Neuroimage **2**, 173–181 (1995).
[98] J. B. Poline, K. J. Friston, K. J. Worsley, and R. S. J. Frackowiak, ''Estimating smoothness in statistical parametric maps: Confidence intervals on *p*-values,'' J. Comput. Assisted Tomogr. **19**, 788–796 (1995).
[99] P. Bandettini, A. Jesmanowicz, E. Wong, and J. Hyde, ''Processing strategies for time-course data sets in functional MRI of the human brain,'' Magn. Reson. Med. **30**, 161–173 (1993).